Newsletters on Stratigraphy, Vol. 55/4 (2022), 451–477
Published online February 18, 2022; published in print September 2022

Carbon- and oxygen-isotope signature of the Toarcian Oceanic Anoxic Event: insights from two Tethyan pelagic sequences (Gajum and Sogno Cores – Lombardy Basin, northern Italy)

Elisabetta Erba[1], Liyenne Cavalheiro[1], Alexander J. Dickson[2,3], Giulia Faucher[1], Gabriele Gambacorta[1]*, Hugh C. Jenkyns[2] and Thomas Wagner[4]

With 11 figures

Abstract. The early Toarcian Oceanic Anoxic Event (T-OAE) was associated with major climatic changes involving profound effects on the global carbon cycle. In this study, we present new carbon- and oxygen-isotope, $CaCO_3$ and total organic carbon (TOC) records from two cores (Sogno and Gajum Cores) that recovered pelagic successions from north-western Tethys. A palaeobathymetry of about 1000 and 1500 m water depth is tentatively reconstructed for the Gajum and Sogno sites, respectively. The investigated sections thereby represent some of the deepest records of the T-OAE in the western Tethys. During the early Toarcian, sedimentation in the Lombardy Basin (Southern Alps, northern Italy) was characterized by the deposition of the Fish Level (Livello a Pesci), a dark grey to black marly claystone with low $CaCO_3$ content and relatively high TOC content. In the two cores, the Fish Level (~5 m and ~15 m-thick at Sogno and Gajum, respectively) is subdivided into three lithostratigraphic intervals: a lower part, with minimum $CaCO_3$ (5–10 %) and TOC (~0.2–0.3 %) values; a central part with a progressive increase in TOC up to ~1.4 %, and an upper part characterized by the highest TOC up to ~2.5 %. Within the Fish Level a lower grey interval and an upper black interval are defined based on lithological features. Carbon-isotope chemostratigraphy resolves a $\delta^{13}C_{carb}$ negative excursion of ~3 ‰ at Sogno and ~6 ‰ at Gajum, and a $\delta^{13}C_{org}$ negative excursion of ~7 ‰ at both locations. This global carbon cycle anomaly, named the 'Jenkyns Event', is here subdivided into a lower J1 and an upper J2 segment. As highlighted by lithostratigraphic evidence, nannofossil biostratigraphy and chemostratigraphic correlations, a hiatus elides part of the succession below the Fish Level in the Gajum Core, although without compromising the completeness of the Fish Level itself. High-resolution $\delta^{13}C$ data indicate that the base of the Fish Level is synchronous, but the top diachronous at the two coring sites. The same synchroneity of the base and diachroneity of the top of the black shale interval is identified in the Umbria-Marche Basin, suggesting that the duration of anoxia was not identical over very modest to relatively long distances.

Key words. T-OAE, Toarcian, C- and O-stable isotopes, chemostratigraphy, black shales

Authors' addresses:
[1] Dipartimento di Scienze della Terra "A. Desio", Università degli Studi di Milano, Via Mangiagalli 34, 20133, Milan, Italy
[2] Department of Earth Sciences, University of Oxford, South Parks Road, Oxford, OX1 3AN, U.K.
[3] Department of Earth Sciences, Royal Holloway University of London, Egham, Surrey, TW20 0EX, U.K.
[4] The Lyell Centre, School of Energy, Geoscience, Infrastructure and Society, Heriot-Watt University, Edinburgh, EH14 4AS, U.K.
* Corresponding author: gabriele.gambacorta@guest.unimi.it

DOI: 10.1127/nos/2022/0690 Borntraeger Science Publishers, Stuttgart, www.borntraeger-cramer.com

1. Introduction

The Toarcian Oceanic Anoxic Event (T-OAE) represents an episode of globally distributed anoxia with extensive accumulation of organic matter from coastal to pelagic settings (Jenkyns 1985, Jenkyns 1988, Jenkyns 2010). Release of high amounts of CO_2 are interpreted as triggers of extreme palaeoenvironmental change. Possible sources of greenhouse gases are related to the degassing of the Karoo–Ferrar large igneous province (Percival et al. 2015, Heimdal et al. 2021) and/or dissociation of methane hydrates along continental margins and/or terrestrial environments (Hesselbo et al. 2000, Pálfy and Smith 2000, McElawin et al. 2005, Svensen et al. 2007, Percival et al. 2015, Them et al. 2017, Ruebsam et al. 2019). Under greenhouse climatic conditions, an accelerated hydrological cycle, with enhanced continental weathering favoured by the elevated concentrations in atmospheric carbon dioxide, led to increased nutrient input into the oceans (Cohen et al. 2004, Jenkyns 2010, Percival et al. 2016, Izumi et al. 2018, Kemp et al. 2020).

The T-OAE, originally recognized due to the globally distributed record of a coeval lower Toarcian black shale (Jenkyns 1985), is associated with a negative carbonate and organic-carbon isotope anomaly measured both in terrestrial (lacustrine), shallow- and deep-marine archives, including sediments from the ancestral Pacific Ocean (Jenkyns and Clayton 1986, Hesselbo et al. 2000, Hesselbo et al. 2007, Schouten et al. 2000, Röhl et al. 2001, Jenkyns et al. 2001, Jenkyns et al. 2002, McElwain et al. 2002, Kemp et al. 2005, Emmanuel et al. 2006, van Breugel et al. 2006, Sabatino et al. 2009, Al-Suwaidi et al. 2010, Caruthers et al. 2011, Gröcke et al. 2011, Hesselbo and Pieńkowski 2011, Kafousia et al. 2011, Kafousia et al. 2014, Izumi et al. 2012, Trabucho-Alexandre et al. 2012, Reolid 2014, Xu et al. 2017, Them et al. 2017, Fantasia et al. 2018, Ikeda et al. 2018, Filatova et al. 2020, Reolid et al. 2020, Ruebsam and Al-Husseini 2020, Remirez and Algeo 2020, Hougård et al. 2021).

Long time-series show that this negative isotope excursion intersects an overarching positive excursion extending over much of the lower Toarcian (Jenkyns and Clayton 1997, Jenkyns 2003, Xu et al. 2018, Storm et al. 2020). Thermogenic methane associated with metamorphism of organic-rich sediment, dissociation of marine or terrestrial clathrates, and volcanogenic CO_2 have been variously credited with causing the observed negative carbon-isotope anomaly; the extensive broad positive carbon-isotope excursion is attributed to accelerated global marine and lacustrine carbon burial (Jenkyns 1988, Jenkyns 2010, Fantasia et al. 2018, Xu et al. 2018).

Both strontium-isotope ($^{87}Sr/^{86}Sr$) and osmium-isotope ($^{187}Os/^{188}Os$) anomalies have also been documented as evidence of accelerated continental weathering in response to a global climate change (Jenkyns 2003, Jenkyns 2010, Cohen et al. 2004, Ullmann et al. 2013, Percival et al. 2016, Them et al. 2017, Jenkyns and Macfarlane 2021) with extraordinary warmth (Dera et al. 2011, Korte and Hesselbo 2011, Gómez et al. 2016, Ruebsam et al. 2020) associated with a major marine transgression (Hallam 1981, Haq et al. 1987, Hardenbol et al. 1998). Available records suggest that, in addition to anoxia, these extreme conditions triggered a biocalcification crisis (Erba 2004, Mattioli et al. 2004, Tremolada et al. 2005, Casellato and Erba 2015, Erba et al. 2019a, Reolid et al. 2020), enhanced primary productivity (Erba 2004, Jenkyns 2010), and ocean acidification (Erba 2004, Trecalli et al. 2012, Casellato and Erba 2015, Posenato et al. 2018, Müller et al. 2020, Ettinger et al. 2021).

New carbon- and oxygen-isotope data calibrated against nannofossil biostratigraphy are presented from two Italian pelagic sequences of latest Pliensbachian–early Toarcian age cored in the Lombardy Basin (Southern Alps, northern Italy) (Fig. 1). Excellent recovery of the Sogno and Gajum Cores (Erba et al. 2019b) provided high-quality material for this study. The estimated palaeowater depth of the selected pelagic sites ranges from 1000–2000 m (Gaetani and Poliani 1978), thereby representing some of the deepest records known of the T-OAE and potentially offering new insights into the dynamics of the Tethyan deep carbonate system under environmentally perturbed conditions. The primary objective of this account is to utilize the detailed characterization of the

Fig. 1. A. and B. Present-day location of the Sogno and Gajum drilling sites. C. Present-day map of the Lombardy area. D. Palaeogeographic location of the studied successions during the Toarcian (~180 Ma) (modified after Scotese 2011). E. Early Toarcian palaeogeographic map of the western Tethys and European epicontinental sea (modified after Fantasia et al. 2019). F. Schematic section across the Lombardy Basin during the Jurassic (modified after Bernoulli et al. 1979). The palaeo-locations of the two studied sites are indicated.

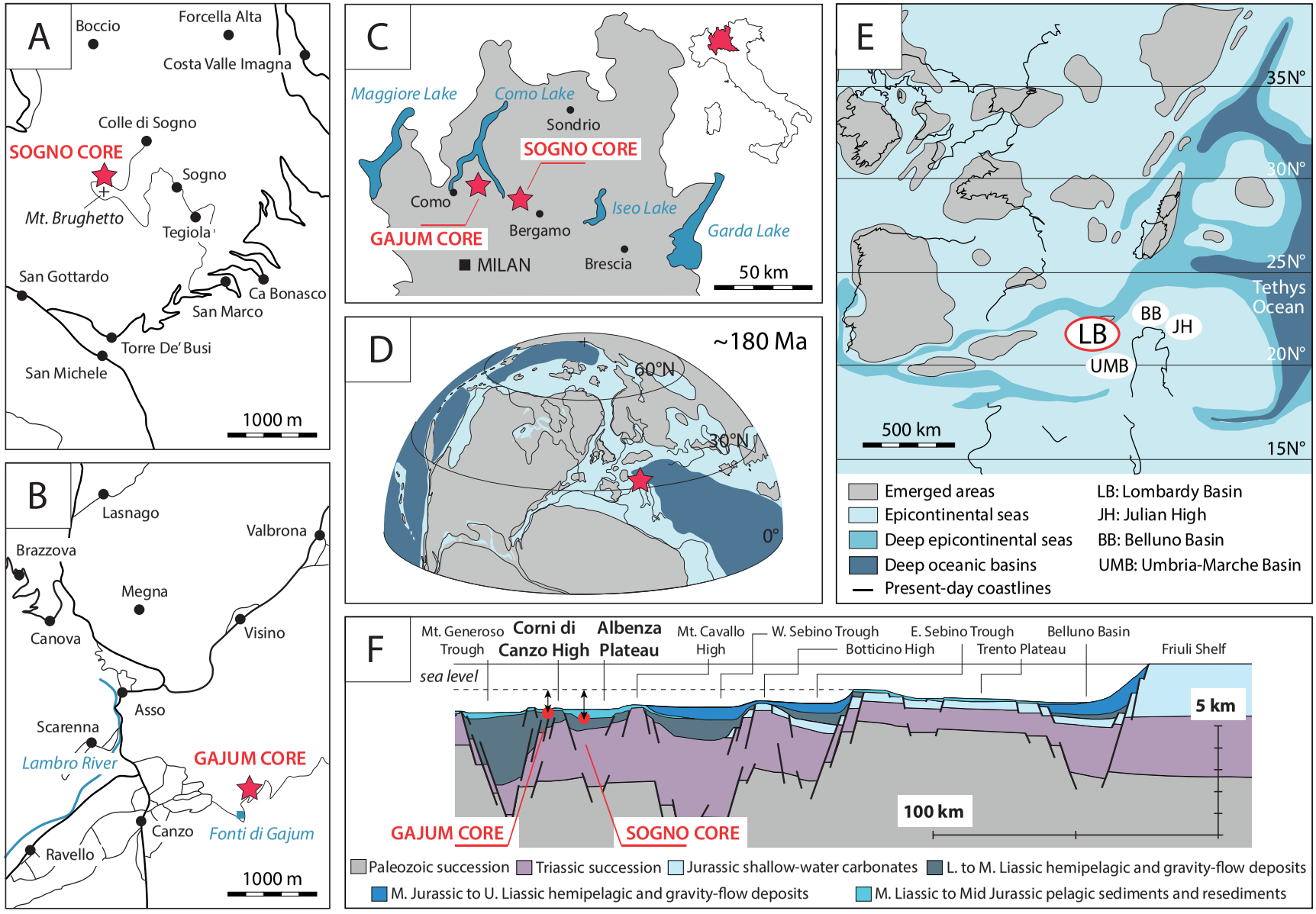
A
Boccio
Forcella Alta
Costa Valle Imagna
Colle di Sogno
SOGNO CORE
Sogno
Mt. Brughetto
Tegiola
San Gottardo
Ca Bonasco
San Marco
Torre De' Busi
San Michele
1000 m
B
Lasnago
Valbrona
Brazzova
Megna
Canova
Visino
Asso
Scarenna
Lambro River
GAJUM CORE
Canzo
Fonti di Gajum
Ravello
1000 m
C
Maggiore Lake
Como Lake
Sondrio
SOGNO CORE
Como
Iseo Lake
Bergamo
Garda Lake
GAJUM CORE
MILAN
Brescia
50 km
D
~180 Ma
60°N
30°N
0°
E
35N°
30N°
25N°
Tethys Ocean
BB
JH
LB
UMB
20N°
500 km
15N°
Emerged areas
Epicontinental seas
Deep epicontinental seas
Deep oceanic basins
Present-day coastlines
LB: Lombardy Basin
JH: Julian High
BB: Belluno Basin
UMB: Umbria-Marche Basin
F
Mt. Generoso Trough
Corni di Canzo High
Albenza Plateau
Mt. Cavallo High
W. Sebino Trough
Botticino High
E. Sebino Trough
Trento Plateau
Belluno Basin
Friuli Shelf
sea level
5 km
100 km
GAJUM CORE
SOGNO CORE
Paleozoic succession
Triassic succession
Jurassic shallow-water carbonates
L. to M. Liassic hemipelagic and gravity-flow deposits
M. Jurassic to U. Liassic hemipelagic and gravity-flow deposits
M. Liassic to Mid Jurassic pelagic sediments and resediments

carbon-isotope stratigraphy of the T-OAE in the Lombardy Basin to investigate the causes and consequences of this major environmental perturbation. In particular, the identification of local/regional versus global isotopic signals should allow the disentangling of small-scale changes from global forcing functions that influenced the ocean/atmosphere system.

2. Geological setting

The Lombardy Basin, located in northern Italy (Fig. 1A), was part of the relatively undeformed portion of the continental margin of the Adria microplate in the western Tethys Ocean (Gaetani 2010) (Figs. 1B and 1C). A latest Triassic–earliest Jurassic multiphase rifting, associated with some environmental change, disrupted a relatively continuous carbonate-platform belt producing an articulated "horst and graben" bathymetry in a pelagic setting (Bernoulli and Jenkyns 1974, Bernoulli and Jenkyns 2009, Winterer and Bosellini 1981, Bosence et al. 2009, Santantonio and Carminati 2011, Jenkyns 2020). This palaeogeographic configuration is clearly documented by different sedimentary regimes with deeper zones characterized by thick relatively complete successions, whereas typically condensed and incomplete sequences accumulated on structural highs (Gaetani 1975, Gaetani 2010). During the Early Jurassic the Lombardy Basin became a relatively deep, fully pelagic area between the Lugano High to the west and the Trento Plateau to the east, further subdivided into a number of troughs and palaeohighs that are, from west to east: Monte Nudo Trough, Lugano High, Generoso Trough, Corni di Canzo High, Albenza Plateau, Monte Cavallo High, Sebino Trough, Botticino High (Fig. 1F). Slopes connecting structural highs to troughs were marked by slumps, resedimented bodies, and, locally, megabreccias (Castellarin 1972, Gaetani and Erba 1990, Pasquini and Vercesi 2002, Gaetani 2010).

During the early Toarcian, sedimentation in the Lombardy Basin was characterized by the deposition of the so-called Fish Level (Livello a Pesci) (Tintori 1977, Gaetani and Poliani 1978, Erba and Casellato 2010, Erba et al. 2019a), a typically 0.5 to 5 m-thick dark grey to black marly claystone interval, with a thickness of up to few tens of metres in the most expanded sections.

The Sogno Core (45°47'20.5" N, 9°28'30.0" E) (Erba et al. 2019b) was drilled next to the outcropping type-section of the Sogno Formation (Gaetani and Poliani 1978), along the road SP 179 on the northern slope of Monte Brughetto (Gaetani and Poliani 1978, Jenkyns and Clayton 1986, Gaetani and Erba 1990, Hinnov et al. 2000, Muttoni et al. 2005, Channell et al. 2010, Casellato and Erba 2015) (Fig. 1A). The lower Toarcian portion of the Sogno Formation, no longer well exposed, consists of about 24 metres of varicoloured limestones and marlstones, with calcareous claystones as minor lithologies overlying the grey, more massive Domaro Limestone Formation, about a metre of which was recovered in the bottom part of the core (Fig. 2). The cored Fish Level (*sensu* Gaetani and Poliani 1978) consists of ~5 m of dark grey to black marly claystones. In particular, following the lithostratigraphy of Erba et al. (2019b), within the Fish Level three intervals are distinguished from bottom to top: an interval consisting of grey to very dark grey and dark red clayey marlstones (Unit 7); grey to very dark grey clayey marlstones with reddish to greyish spots (Unit 6); black shales characterized by well-developed lamination and pyrite nodules (Unit 5).

The Gajum Core (45° 51' 3.2" N, 9° 17' 19.5" E) (Erba et al. 2019b) was drilled close to "Fonte Gajum" located east of Canzo (CO), in a lateral incision of the Ravella Valley next to the trail named Via delle Alpi (Fig. 1B). The marly limestones, marlstones and clayey marlstones of the Sogno Formation (about 22.5 metres) are separated from the underlying Domaro Limestone Formation (about 4 metres) by a sharp undulated lithological contact and overlain by about 1.5 metres of reddish nodular limestones of the Rosso Ammonitico Lombardo Formation (Fig. 3). The Fish Level in the Gajum Core is more expanded than in the Sogno Core, with a thickness of about 16 metres *versus* 5 metres, respectively. Following the lithostratigraphy of Erba et al. (2019b), three units are distinguished within the Fish Level, from bottom to top: an interval consisting of dark grey to very dark grey to black marly claystones, with evident laminations and local faint bioturbated patches (Unit 6); dark to very dark grey to black clayey marlstones interrupted by four intervals of dusky red limy cherts with a few levels characterized by green-coated limy-chert nodules (Unit 5); dark to very dark grey to black marly claystones with evident lamination and common pyrite nodules (Unit 4).

Figure 4 illustrates the lithological variations detected within the Fish Level at Sogno and Gajum showing two distinctive parts, namely a lower grey interval and an upper black interval. The latter is lithologically similar at the two sites, being character-

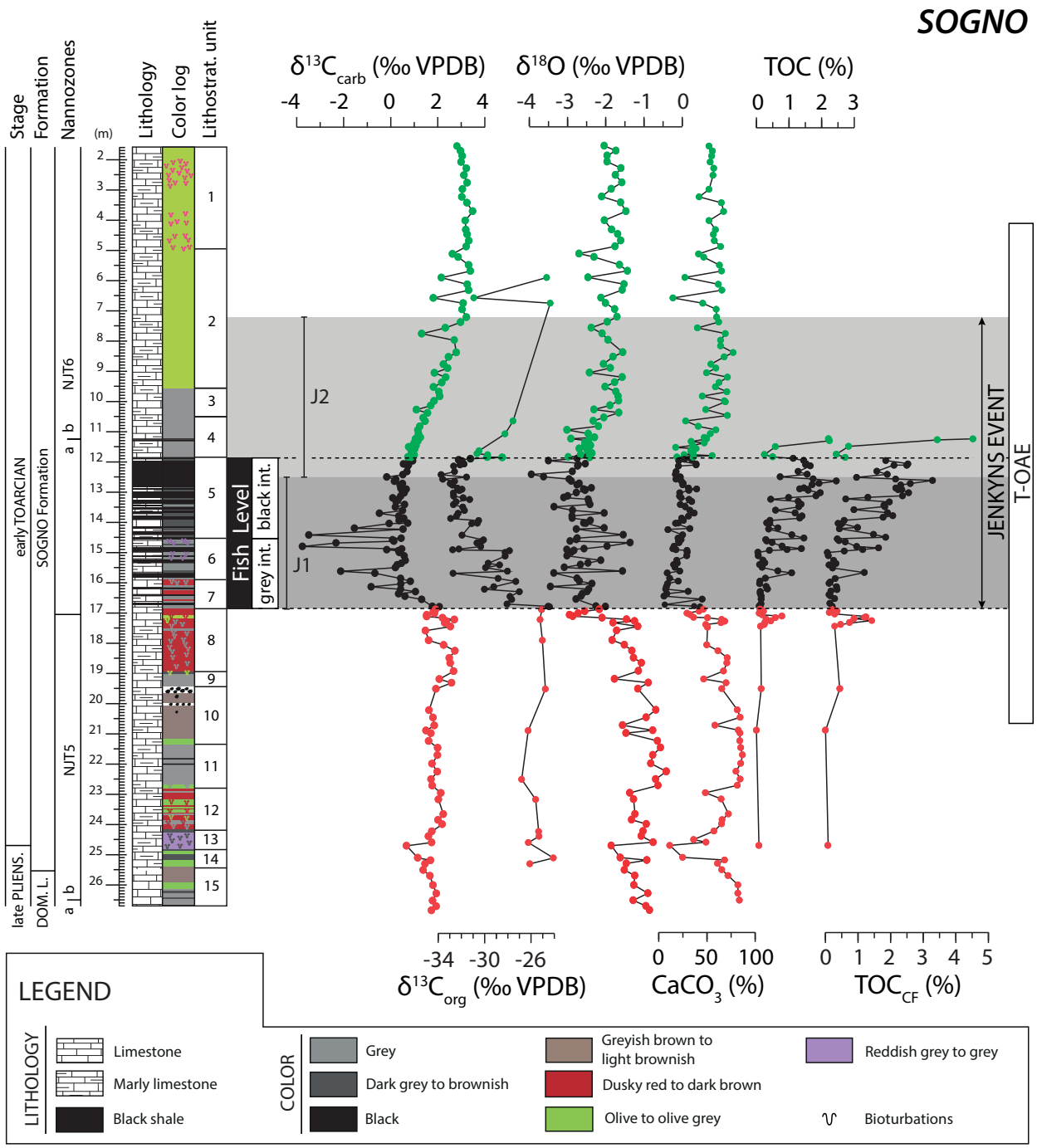

Fig. 2. Nannofossil biostratigraphy, lithostratigraphy, isotopic records ($\delta^{13}C_{carb}$, $\delta^{13}C_{org}$ and $\delta^{18}O_{carb}$), $CaCO_3$ content, total organic carbon (TOC), and total organic carbon on a carbonate-free basis (TOC_{CF}) of the Sogno Core. Nannofossil biostratigraphy from Visentin and Erba (2021); lithostratigraphy and $CaCO_3$ from Erba et al. (2019b). Samples below, within and above the Fish Level are indicated in red, black and green, respectively. The lower part (J1) and the upper part (J2) of the lithostratigraphic expression of the Jenkyns Event are highlighted with a dark grey and a light grey band, respectively (see text for explanation).

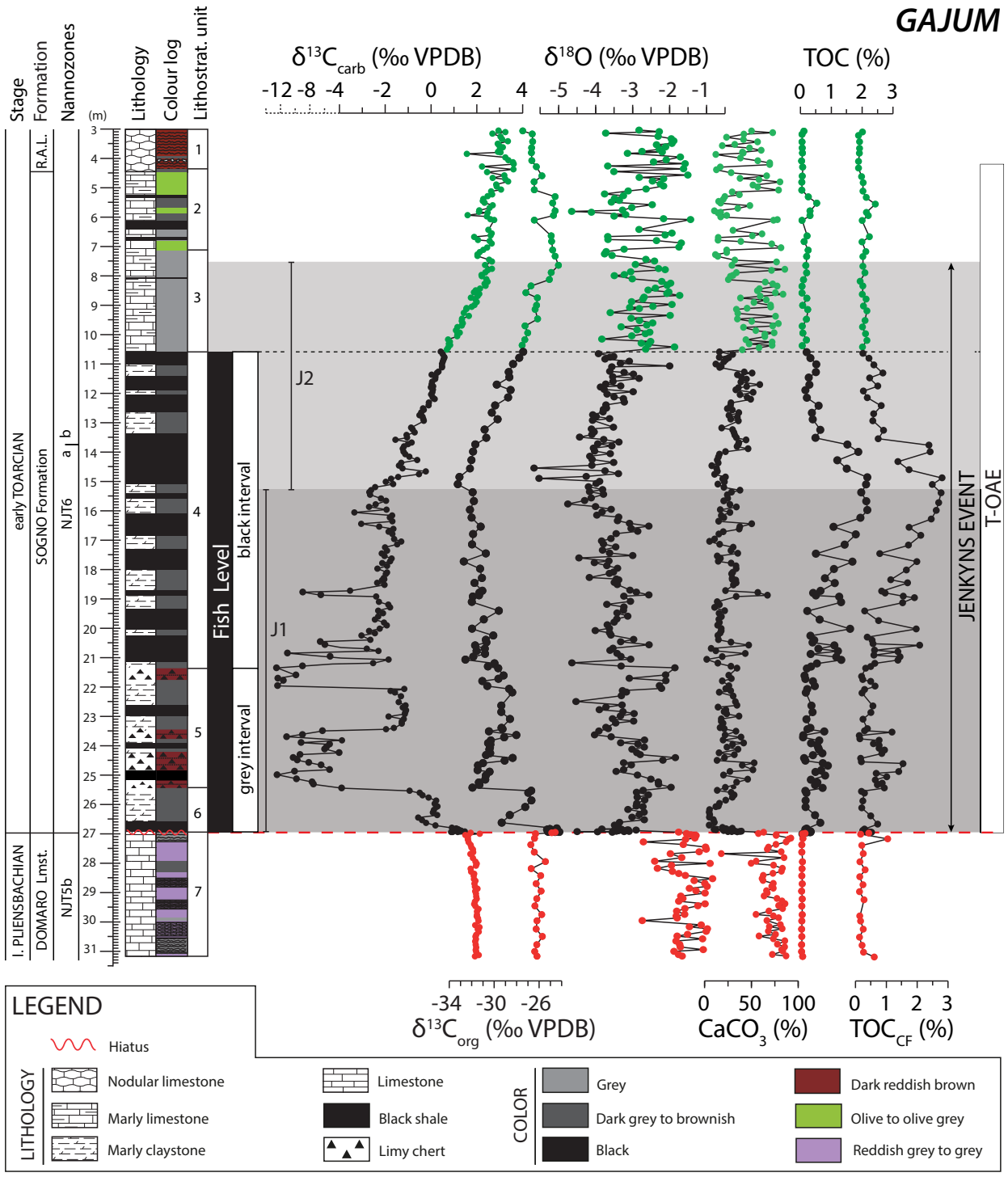

Fig. 3. Nannofossil biostratigraphy, lithostratigraphy, isotopic records ($\delta^{13}C_{carb}$, $\delta^{13}C_{org}$ and $\delta^{18}O_{carb}$), $CaCO_3$ content, total organic carbon (TOC), and total organic carbon on a carbonate-free basis (TOC_{CF}) of the Gajum Core. Nannofossil biostratigraphy from Visentin and Erba (2021); lithostratigraphy and $CaCO_3$ from Erba et al. (2019b). The hiatus at the base of the Fish Level is indicated by a red dashed line (see text for explanation). Samples below, within and above the Fish Level are indicated in red, black and green, respectively. For the sake of readability, lower $\delta^{13}C_{carb}$ values are reported using a different scale. The lower part (J1) and the upper part (J2) of the lithostratigraphic expression of the Jenkyns Event are highlighted with a dark grey and a light grey band, respectively (see text for explanation).

ized by laminated fissile black shales, rich in pyrite powder and nodules, and very dark grey, homogenous to faintly bioturbated marly claystones. The lower grey interval, by contrast, predominantly consists of grey and bioturbated marly claystones with different intercalations of reddish lithologies. Whereas in the Sogno Core dusky red clayey marlstones characterize the lowermost part of the Fish Level (Unit 7 in Fig. 2), in the Gajum Core distinctive dark reddish brown limy chert levels occur in the upper part of the grey interval (Unit 5 in Fig. 3). Peculiar emerald-coloured mm-thick laminae are present at 14.69 and 15.28 m within Unit 6 in the Sogno Core (Fig. 4). In the Gajum Core, mm- to cm-sized pea-green coated nodules are documented in the dark red limy chert layers between 23.42 and 23.81 m and between 24.36 and 24.44 m (Fig. 4).

The Sogno and Gajum sites were located in quite different geological settings within the Lombardy Basin, on a pelagic plateau (Albenza Plateau) and in an inner basin along the slope of a structural high (Corni di Canzo Mt.), respectively (Gaetani and Erba 1990, Pasquini and Vercesi 2002, Gaetani 2010) (Fig. 1F). The Late Jurassic palaeobathymetry of the Southern Alps reconstructed by Bernoulli et al. (1979) potentially provides some estimates of the former water depths of the Sogno and Gajum sites (Fig. 1F). However, these Late Jurassic depth estimates are in no way rigorously quantitative since they rely on regional stratigraphy, sedimentary geometry and thicknesses of the sequences together with the assumed palaeobathymetric significance of characteristic pelagic facies, as suggested by Bosellini and Winterer (1975). Gaetani (2010) detailed the Jurassic evolution of the Southern Alps as part of a passive continental margin adjacent to a spreading centre. The differential subsidence driven by the extensional regime was largely over by late Aalenian times, subsequently becoming more evenly distributed, as documented by the sedimentary successions in various portions of this Tethyan margin (Winterer and Bosellini 1981, Bernoulli and Jenkyns 1974, Bernoulli and Jenkyns 2009, Gaetani 2010). Consequently, following Jenkyns (1988), the position of Early Jurassic sea level can be equated to the top of the Trento Plateau that remained a shallow-water carbonate platform during the Hettangian–earliest Toarcian time interval, allowing an estimate of the palaeowater depths of troughs and highs within the adjacent Lombardy Basin. In this way, the palaeowater

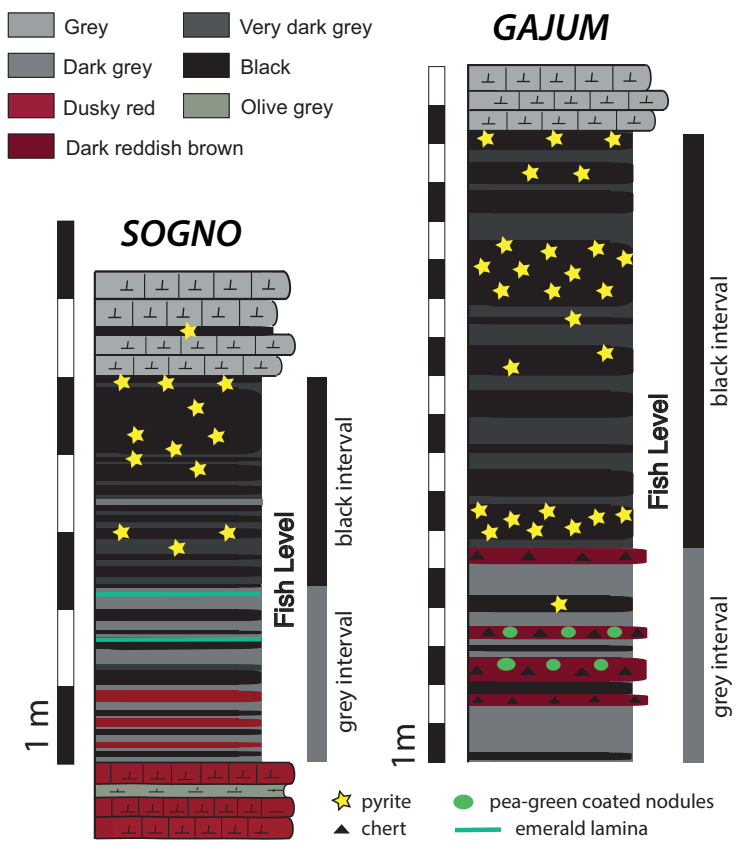

Fig. 4. Detailed lithostratigraphy of the Fish Level in the Sogno and Gajum Cores. Two distinctive parts, namely a lower grey interval and an upper black interval are distinguished. See text for details.

depths of the Sogno and Gajum sites are tentatively reconstructed to be about 1500 and about 1000 metres, respectively, during the Early Jurassic.

Generally, the palaeobathymetry of Early Jurassic basins in the southern part of the Tethyan area is poorly quantified. Excluding shallow-water carbonate platforms (e. g., Woodfine et al. 2008, Sabatino et al. 2009, Ettinger et al. 2021), information on water depths for pelagic–hemipelagic settings is scarce, although the reconstructions of Winterer (1998) for the eastern Lombardy Basin (Sebino Trough, Fig. 1F) suggests comparable palaeodepths to those suggested here for the Sogno and Gajum sites. A quantitative water-depth estimate for the Peniche section (Portugal) was given by Bjerrum et al. (2001), who proposed a figure of about 200 m for the shallow westerly dipping homoclinal ramp of the Lusitanian Basin. At the other extreme, the occurrence of radiolarites stratigraphically associated with organic-rich T-OAE shales in the Pindos Zone (northern Peloponnese, Greece) was used to suggest, for the so-called Kastelli Pelites, a water depth greater than that of typical Tethyan continental margins (Kafousia et al. 2011). This example apart, the investigated Sogno and Gajum sites provide some of the deepest records of the T-OAE to complement the information already available for shallower sites in the Tethyan region.

There has been a similar reticence in the literature to giving estimates for the depositional palaeodepths of T-OAE successions in the shelf seas of northern Europe, although studies of relative sea-level change during the Toarcian are relatively plentiful (e. g., Hesselbo and Jenkyns 1998, Röhl and Schmid-Röhl 2005). An overall stratigraphic association with current-bedded clastic sediments of various facies-types, as well as the local presence of silt-grade sedimentary structures in the black shales themselves, likely precludes deposition of the organic-rich sediments in great water depths (e. g., Trabucho-Alexandre et al. 2012). However, the prevailing anoxic to euxinic conditions would have required, during certain intervals at least, the presence of a modestly well-developed and stable water column. Hallam (1967) opted for a relatively shallow 15 to 30 m for the depositional depth of lower Toarcian black shales in Yorkshire, north-east England, whereas Frimmel et al. (2004) and Röhl et al. (2001) suggested figures of ~50 m and 100–150 m, respectively, for coeval facies in south-west Germany. The greater figures seem intrinsically more reasonable given the overall tectonic context of a shelf region undergoing crustal extension and subsidence accompanied by a regional sea-level rise. In any event, the contrast in proposed palaeobathymetry when compared with Tethyan pelagic facies in the Lombardy Basin is clear.

3. Material and methods

3.1. Carbonate carbon and oxygen isotopes

A total of 173 bulk dried and ground samples of the Sogno Core (one sample every ~10–15 cm) were measured for carbon and oxygen stable isotopes. Measurements were performed at the Open University (U.K.) using a Thermo Delta-Plus Advantage mass spectrometer attached to a Thermo GasBench. Samples were reacted with phosphoric acid (H_3PO_4) at 60 °C. Data were corrected to the VPDB scale with a linear two-point calibration using NBS-18 and NBS-19 (n = 3 each) and an in-house Maastrichtian limestone. Reproducibility of replicated standards is better than ±0.1 ‰ for $\delta^{13}C_{carb}$ and $\delta^{18}O_{carb}$.

A total of 342 bulk dried and ground samples of the Gajum Core (one sample every 5–10 cm) were measured for stable carbon and oxygen isotopes at the Department of Earth Sciences “A. Desio”, Milan University. Measurements were performed using an automated carbonate preparation device (GasBench II) connected to a Delta V Advantage (Thermo Fisher Scientific Inc.) isotopic ratio mass spectrometer (IRMS). Weighed powders (about 200–1000 µg each depending on sample carbonate content) were reacted with >99 percentage phosphoric acid (H_3PO_4) at 70 °C. The reference materials used for carbon- and oxygen-isotope analyses are the international standards, IAEA 603 and NBS-18. Analytical reproducibility is better than ± 0.1 ‰. Stable-isotope ratios are reported using the conventional δ notation to indicate per mil (‰) deviation from the VPDB standard (Coplen 1994).

3.2. Organic-carbon isotopes

A sub-set of 77 bulk dried samples, principally covering the Fish Level interval of the Sogno Core, were analysed for bulk organic stable carbon-isotope ratios ($\delta^{13}C_{org}$). Samples were crushed with an agate pestle and mortar to <125 µm. Carbonate was removed by treating ~1 g of sample with 20 ml 1 M HCl, and heating on a hot plate for about 2 h. This phase was

repeated until no visible reaction occurred. The acid-treated samples were then washed with distilled de-ionised water three times to achieve a neutral pH, oven dried at 40 °C and re-crushed. A mass of decarbonated powder equivalent to ~20–100 μg C was then weighed into tin capsules for analysis. Measurements were made at the Open University (U.K.) using a Thermo Flash HT Elemental Analyser coupled to a MAT 253 mass spectrometer. Measured $\delta^{13}C$ compositions were corrected to the VPDB scale with a three-point linear calibration using NIST 8572 glutamic acid ($\delta^{13}C$ = –26.39 ‰), IAEA CH-6 sucrose ($\delta^{13}C$ = –10.45 ‰) and L-Alanine ($\delta^{13}C$ = –23.33 ‰), measured in every sample batch. Sample isotopic ratios are reported as per mil deviation from the VPDB international standard (Coplen 1994). Reproducibility of $\delta^{13}C_{org}$, monitored by standard measurements and duplicates, is better than ±0.1 ‰.

For the Gajum Core, a sub-set of 158 bulk dried samples (one sample every ~20 cm) was analysed for $\delta^{13}C_{org}$ at Iso-Analytical, Crewe Cheshire (U.K.). Weighed powdered samples were acidified with 2M HCl (~24 hours), then washed until reaching neutrality and oven-dried at 60 °C. Thereafter, an aliquot of the sample was weighed into a sealed tin capsule, which was loaded into an autosampler and analysed on a Europa Scientific Elemental Analyser – Isotope Ratio Mass Spectrometry (EA-IRMS). The temperature of the furnace was held at 1000 °C and the temperature in the region of the sample reached ~1700 °C. Calibration to the VPDB standard via IAEA-CH-6 sucrose ($\delta^{13}C$ = –10.45 ‰) was made daily using the in-house IA-R001 (wheat flour, $\delta^{13}C$ = of –26.43 ‰), IA-R005 (beet sugar, $\delta^{13}C$ = –26.03 ‰) and IA-R006 (cane sugar, $\delta^{13}C$ = –11.64 ‰) internal standards. Analytical reproducibility is better than ±0.1 ‰.

3.3. Calcium carbonate content ($CaCO_3$)

The calcium carbonate ($CaCO_3$) content of selected samples from both the Sogno (N = 163 samples) and Gajum (N = 342 samples) was measured at the Department of Earth Sciences "A. Desio", Milan University. The $CaCO_3$ content was detected using the Dietrich-Frühling gas volumetric method by measuring evolved CO_2 after acidification of the bulk sample with HCl (see Erba et al. 2019b). $CaCO_3$ results for both the Sogno and Gajum Cores are reported in weight percentage (%) (Figs. 2 and 3).

3.4. Total organic carbon (TOC)

A total of 79 samples of the Sogno Core, mainly from the Fish Level, were measured for total organic-carbon (TOC) content by Rock-Eval Pyrolysis 6 at the Department of Earth Sciences at Oxford University (U.K.). The TOC content of 158 samples of the Gajum Core was analysed along with bulk organic stable carbon isotopes at Iso-Analytical, Crewe Cheshire (U.K.), using a Europa Scientific Elemental Analyser – Isotope Ratio Mass Spectrometry (EA-IRMS). The total ion beam data recorded the percentage carbon of the acid-washed samples and was used to calculate the TOC values after subtracting the weight-loss data (total inorganic carbon = TIC) determined at the acid washing stage: i. e., %TOC =%TC –%TIC. TOC results for both the Sogno and Gajum Cores are reported in weight percentage (%) (Figs. 2 and 3).

Total organic carbon on a carbonate-free basis (TOC_{CF}) was computed in order to compensate for the highly variable $CaCO_3$ content and evaluate possible dilution effects on the measured total organic matter. TOC_{CF} was calculated using the following formula:

$$TOC_{CF} = TOC * \frac{100}{(100 - CaCO_3)}$$

4. Results

4.1. Carbonate carbon and oxygen isotopes

Carbonate carbon isotopes of the Sogno Core range between 3.5 ‰ and –3.8 ‰ (Fig. 2). In the upper Domaro Limestone and the lower Sogno Formation, carbon isotopes are relatively stable with average values of 1.9 ‰ between 26.83 m and 17.22 m. The carbon-isotope chemostratigraphy shows a minor but distinctive negative anomaly previously identified at the Pliensbachian/Toarcian boundary (Littler et al. 2010, da Rocha et al. 2016) at 24.69 m in the lowermost part of the Sogno Formation. Although in previous studies the base of the Toarcian has been placed at the base of the Sogno Formation (Gaetani and Poliani 1978, Casellato and Erba 2015) we believe that, in the Sogno Core, this stage boundary should be placed at the $\delta^{13}C_{carb}$ minor anomaly as documented at the Peniche GSSP (da Rocha et al. 2016) (Fig. 2). Just below the base of the Fish Level, $\delta^{13}C_{carb}$ values decrease sharply to 0.3 ‰, between 17.22 m and

16.36 m, and remain on average around 0.4 ‰ to about 12.51 m. Notably, negative spikes ranging from –0.5 to –3.7 ‰ occur between 16.13 m and 13.70 m. Starting from the topmost part of the Fish Level, the $\delta^{13}C_{carb}$ record gradually increases towards positive values (12.51–6.33 m) until reaching relatively stable values of about 3 ‰ in the upper part of the cored interval (6.33 m–1.56 m). The pioneering work by Jenkyns and Clayton (1986) first documented a negative C-isotopic interval interrupting a positive excursion in the Sogno outcrop (equal to Monte Brughetto section of Gaetani and Poliani 1978). Although the stratigraphic resolution of the C and O stable isotopic analyses was much lower than in the present study, the values documented by Jenkyns and Clayton (1986) compare well with those derived from the Sogno Core.

In the Sogno Core, oxygen isotopes range between –4.4 ‰ and –0.9 ‰ (Fig. 2), generally showing scattered data. A relatively stable trend is observed from the base of the cored section to the interval just below the base of the Fish Level, documenting average values of –1.7 ‰ between 26.83 m and 17.27 m. Across the Fish Level, $\delta^{18}O_{carb}$ data decrease gradually up to 12.42 m, showing average values of –3.1 ‰. Starting from the topmost part of the Fish Level, oxygen isotopes shift towards positive values (12.42–10.39 m), reaching relatively stable values of about –2.4 ‰ in the upper part of the cored interval between 10.39 m and 1.56 m. As for the $\delta^{13}C_{carb}$ record, the oxygen isotope values obtained for the Sogno Core are fully consistent with data documented for the outcrop (Jenkyns and Clayton 1986).

Carbonate carbon isotopes of the Gajum Core range between 3.6 ‰ and –12.5 ‰ (Fig. 3). In the Domaro Limestone, carbon isotopes are stable around average values of 1.9 ‰ between 31.17 m and 26.96 m. At the contact between Domaro Limestone and the Fish Level, based on high-resolution data (one sample every 0.5–1 cm) $\delta^{13}C_{carb}$ values show a minor increase from 1.5 ‰ to 2.1 ‰ (27.04–27.00 m), followed by a sharp decrease down to –0.6 ‰ at 26.44 m. Above, the carbon-isotope trend continues to a slight decrease across the Fish Level, with average values of about –2 ‰ up to 15.47 m. Notably, in the lower part of the Fish Level, three intervals characterized by a series of very negative values are identified: i) the stratigraphically lowest includes 21 negative data points down to –12.5 ‰ between 25.43 m and 23.51 m; ii) the second occurs between 21.97 m and 20.48 m, and includes 10 very negative data-points down to –12.5 ‰; iii) the uppermost interval consists of three data-points showing values down to –9.0 ‰ between 18.88 m and 18.73 m. Starting from the upper part of the Fish Level, the $\delta^{13}C_{carb}$ curve gradually shifts towards positive values (15.47–7.53 m) reaching relatively stable numbers around 2.7 ‰ in the upper part of the Sogno Formation and lower part of the Rosso Ammonitico Lombardo (7.53–3.08 m).

Oxygen isotopes in the Gajum Core range between –5.7 ‰ and –0.8 ‰, generally showing a large amount of data scatter (Fig. 3). The $\delta^{18}O_{carb}$ values show a relatively stable trend from the base of the cored interval up to the base of the Fish Level, with average values of –1.5 ‰ between 31.17 m and 26.96 m. At the boundary between the Domaro Limestone and the Fish Level, a sharp decrease down to values of about –3 ‰ is documented. Across the Fish Level, $\delta^{18}O_{carb}$ data show a gradual decrease up to 14.57 m, with average values of –3.3 ‰. In the upper part of the Fish Level (14.57–10.53 m), oxygen isotopes start shifting towards higher values returning to relatively stable levels, on average –2.7 ‰, between 10.53 m and 3.08 m.

4.2. Organic-carbon isotopes

Carbon isotopes on bulk organic matter in the Sogno Core range between –33.7 ‰ and –24.1 ‰ (Fig. 2). In the Domaro Limestone and the lower Sogno Formation, $\delta^{13}C_{org}$ results are relatively stable with average values of –25.5 ‰ between 25.29 m and 16.88 m. At the base of the Fish Level, the $\delta^{13}C_{org}$ curve shifts sharply to lower values of –24.4 ‰ to –27.7 ‰ between 16.79 m and 16.55 m. Across the Fish Level, $\delta^{13}C_{org}$ data continue to decrease up to 12.42 m, with average values of –30.8 ‰. Jenkyns and Clayton (1986) provided $\delta^{13}C_{org}$ data for the Fish Level cropping out at Monte Brughetto that are fully consistent with the Sogno Core record, albeit with lower resolution. Starting from the upper part of the Fish Level (12.42 m), $\delta^{13}C_{org}$ data gradually shift towards higher values up to 10.65 m, reaching values up to –28 ‰. In the overlying organic-lean part of the Sogno Formation, only three samples were measured, which are characterized by an average value of –26.6 ‰ between 6.76 m and 5.91 m.

Carbon isotopes on bulk organic matter of the Gajum Core range between –33.3 ‰ and –24.3 ‰ (Fig. 3). In the Domaro Limestone, $\delta^{13}C_{org}$ data are relatively stable around average values of –26.2 ‰ between 31.17 m and 26.96 m. At the contact between the Domaro Limestone and the Fish Level, high-

resolution data show a minor, initial increase from –25 ‰ to –24.4 ‰ (27.00–26.93 m), followed by a sharp and more pronounced decrease down to –29.4 ‰ at 26.53 m. Across the Fish Level, $\delta^{13}C_{org}$ values continue to decrease up to 15.10 m, reaching values of –33.3 ‰. Starting from the upper part of the Fish Level, $\delta^{13}C_{org}$ values gradually increase (15.11–9.48 m), returning to relatively stable levels, on average –25.9 ‰, in the upper part of the Sogno Formation and Rosso Ammonitico Lombardo (9.48–3.08 m).

4.3. Calcium carbonate content ($CaCO_3$)

In the Sogno Core, the calcium carbonate content ranges between 5.5 % and 87.0 % (Fig. 2). In the upper Domaro Limestone and lower part of the Sogno Formation, the $CaCO_3$ content is on average 62.9 % between 26.83 m and 16.88 m. However, a sharp decrease, down to 11.4 %, is documented between 26.00 m and 24.69 m. $CaCO_3$ values decline from just below the base of the Fish Level, with a minimum of about 5 % in the lower Unit 7. In the Fish Level, the calcium carbonate content remains low, with average values of 23.5 % comparable to those documented by Jenkyns and Clayton (1986) for the Monte Brughetto outcrop. $CaCO_3$ starts to rise again above the Fish Level, showing average values of 51.8 % in the upper part of the Sogno Core, between 11.86 m and 1.56 m. However, some fluctuations in the order of about 20–30 % are observed in this interval.

The calcium carbonate content of the Gajum Core ranges between 2.4 % and 92.3 % (Fig. 3). In the Domaro Limestone, the $CaCO_3$ values are on average 73 % between 31.17 m and 26.96 m. At the base of the Fish Level, $CaCO_3$ values sharply decrease down to ~10 % in the lower part of Unit 6. In the Fish Level, between 26.96 m and 10.60 m, the calcium carbonate content remains low with average values of 25.9 %. Above the Fish Level, the calcium carbonate content rises gradually to average values of 46.9 % in the upper part of the Sogno Formation and the Rosso Ammonitico Lombardo, between 10.60 m and 3.08 m. However, fluctuations up to 40 % are documented in this upper interval of the Gajum Core.

4.4. Total organic carbon (TOC)

The TOC values of the Sogno Core fall between 0 % and 2.5 % (Fig. 2). In the lower part of the Sogno Formation, below the Fish Level, TOC content is on average 0.2 % between 24.69 m and 16.88 m, and increase to about 0.8 % just below the base of the Fish Level at ~17.1 m. In the lowermost part of the Fish Level (Unit 7) TOC values are very low (0.2 %). Within lithological Unit 6, TOC starts to increase at 15.6 m reaching values up to ~1.4 %, with an average of 0.5 %. The uppermost part of the Fish Level (Unit 5) is characterized by the highest TOC values, on average 1.3 %, with peaks up to 2.5 %. These data are fully consistent with the TOC values obtained by Jenkyns and Clayton (1986) for the outcropping Fish Level. The interval immediately above the Fish Level is characterized by low values in the lowermost part (~0.4 %), followed by two samples with TOC content of ~2.2 %.

In the Gajum Core, the TOC values range between 0 % and 2.2 % (Fig. 3). In the Domaro Limestone (31.17–26.96 m), the TOC content is stable and extremely low, on average about 0.1 %. The lowermost and central lithostratigraphical units of the Fish Level (Units 6 and 5) are characterized by rather stable low values of about 0.3 % and 0.4 %, respectively. Unit 4 is characterized by a lowermost part (21.39–13.74 m) marked by a progressive increase in TOC up to 2.2 % (average of 1.1 %) and an upper part (13.74–10.60 m) with a low TOC content of ~0.4 %. In the upper part of the Gajum Core above the Fish Level and in the Rosso Ammonitico Lombardo (10.60–3.08 m), TOC values are very low, on average 0.1 %. Only a limited increase is observed in the interval between 5.95 and 5.31 m with an average value of ~0.3 % and a maximum of ~0.5 % at 5.53 m.

5. Discussion

5.1. The Fish Level in the Sogno and Gajum Cores

The Fish Level was originally described by Tintori (1977) in the section cropping out south of Monte Brughetto as a 1.75 m-thick interval consisting of fissile, brownish to black claystones and clayey marlstones, with planar alignments of small pyritic crystals. Gaetani and Poliani (1978) established the type section of the Sogno Formation on the road north of Monte Brughetto and described, in the middle part of lithozone 1, a 4.3 m-thick clayey interval containing common fish remains. According to Gaetani and Poliani (1978), the Fish Level *sensu stricto* can reach a thickness of 50 cm and is present only in the most

expanded sequences. However, the precise position of the Fish Level in the Colle di Sogno reference section or in other localities was not defined and, consequently, Casellato and Erba (2015) applied the name to the entire clayey interval of Gaetani and Poliani (1978). The same criteria were followed by Erba et al. (2019b) for the identification of the Fish Level in the Sogno and Gajum Cores, and used to identify the lithostratigraphic signature of the T-OAE, as suggested by Jenkyns (1985 1988).

The detailed sedimentological characterization of the Fish Level recovered with the Sogno and Gajum Cores was used to identify a lower grey interval and an upper black interval (Figs. 2, 3, and 4). The variable thickness of these two intervals as well as of the total thickness of the Fish Level appears dependent on the location within specific morphostructural features of the Lombardy Basin. It is worthwhile noting that the upper black interval is lithologically similar in the two cores, whereas the lower grey interval is rather variable. Most probably the Fish Level reported by Tintori (1977) corresponds to the sole upper black interval that should therefore be considered the Fish Level *sensu stricto*.

The expanded nature of the Fish Level in the Sogno and Gajum Cores offers the opportunity to investigate in detail the lithostratigraphic variations associated with the C-isotope anomaly. At both sites, the Fish Level base and top are identified as corresponding with the lowermost and uppermost dark grey to black shale, respectively (Erba et al. 2019b). Nevertheless, the Fish Level basal and top contacts are different in the two cores. Notably, in the Sogno Core the upper boundary corresponds to the top of the continuous black-shale interval overlain by grey marlstones, whereas the base is fixed at the bottom of the lowermost dark grey marlstone overlying a reddish interval (Unit 8). As described above (Fig. 4), the basal part of the Fish Level (Unit 7) is developed as greyish marly claystones with a few black shales, but also some reddish levels. On the contrary, in the Gajum Core the base of the Fish Level is well defined due to the abrupt occurrence of black shales, whereas the top is characterized by a transition from black shales to progressively dark grey to grey marly claystones and marlstones (Figs. 2, 3, and 4). The sharp lithological nature of the lower boundary of the Fish Level in the Gajum Core is related to the occurrence of a hiatus that may cover ~600 kyrs based on nannofossil biostratigraphy (Visentin and Erba 2021). Indeed, from a lithological point of view, the hiatus coincides with the boundary between light grey limestones of the Domaro Limestone Formation and the grey interval of the Fish Level, thereby eliding the lowermost Toarcian part of the Sogno Formation. Moreover, as illustrated in Figure 5, the uppermost centimetres of the Domaro Limestone are characterized by a pseudo-nodular facies and an undulating surface with the overlying grey interval of the Fish Level. However, calcareous nannofossil biostratigraphy and geochemical data suggest that the basal part of the Fish Level is most probably complete.

The hiatus detected at the base of the Fish Level is interpreted as the result of downslope sediment (mass) transport as documented by megabreccia bodies occurring in various palaeo-locations near to the Gajum drillsite, at the foot or in lower parts of the slopes of the Mt. Corni di Canzo palaeohigh (Gaetani and Erba 1990, Pasquini and Vercesi 2002). Sedimentary discontinuities of similar age and duration have been documented for several lower Toarcian sections from the Lusitanian Basin as well as in Western Tethyan sections and have been ascribed to rapid regression/transgression phases around Pliensbachian/Toarcian boundary time, in the earliest *polymorphum* Zone and immediately before the T-OAE negative CIE: some authors have attributed such putative sea-level oscillations to glacio-eustatic control (Pittet et al. 2014). A rapid glacio-eustatic sea-level fall preceding the T-OAE negative CIE was also suggested, based on the presence of deeply incised valleys in marine sections exposed in Greenland and Morocco (Krencker et al. 2019). However, the palaeowater depth of the Gajum site (about 1000 m) excludes a similar cause for the hiatus dated in this core. This contention is further reinforced by the occurrence of continuous and complete sequences in several parts of the Lombardy Basin, as at Sogno on the Albenza Plateau. Rather, an early Toarcian tectonic phase associated with the rifting that propagated eastwards in the Southern Alps during the Late Triassic (Norian) to Middle Jurassic, was responsible for gaps and massive re-sedimentation in various parts of the Lombardy Basin (Gaetani 2010).

Despite the lithostratigraphical differences, related to the specific palaeo-physiography of the Gajum (Corni di Canzo High) and Sogno (Albenza Plateau) sites, some common geochemical features are observed within the Fish Level in the Sogno and Gajum Cores. The lower part of the grey interval, with minimum $CaCO_3$ values (5–10 %) and TOC (~0.2 %), is characterized by bioturbated, grey to very dark grey, and dark red marlstones in the Sogno Core (Unit 7) and bioturbated, dark grey to very dark

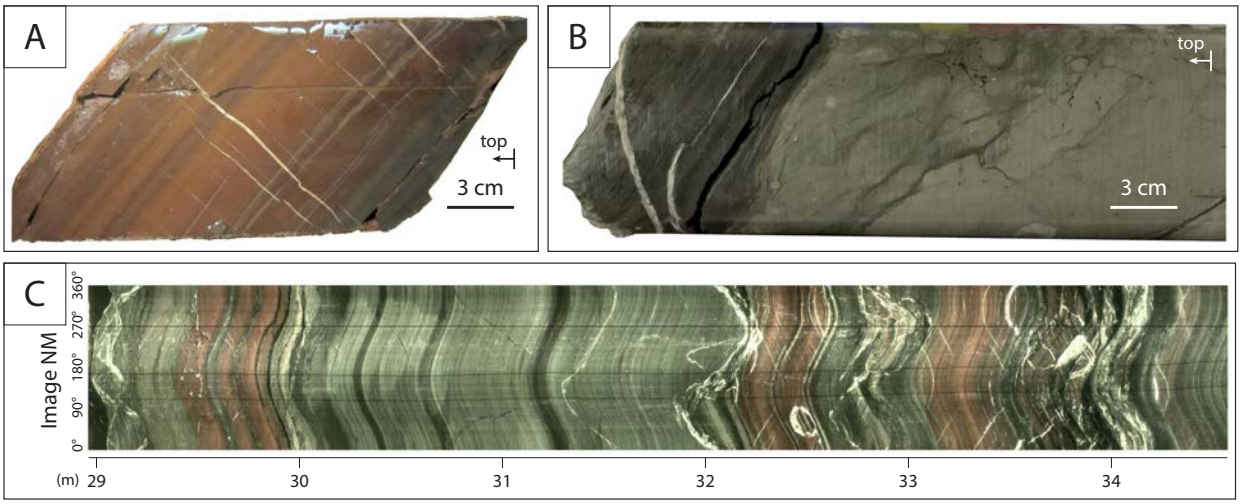

Fig. 5. A. Dusky red limy chert interval in the Gajum Core (slabbed core 22; ~32.4 m, – penetration depth, ~23.7 m – stratigraphic depth). B. Boundary between the Domaro Limestone (on the right) and Sogno Formation (on the left) (core 25; ~36.78 m, – penetration depth, ~26.95 m – stratigraphic depth). An undulated surface marks the sharp boundary between the pseudo-nodular limestones and the Fish Level. C. Gajum borehole well image (from ~29 to ~34.5 m – penetration depth; from ~21 to ~25.3 m – stratigraphic depth). Three intervals of dusky red limy cherts interspersed with the grey to black marly claystones can be observed.

grey marly claystones in the Gajum Core (Unit 6). At Sogno, the onset of the Fish Level is marked by a drop in $CaCO_3$ associated with the "*Schizosphaerella* crisis" (Erba 2004, Casellato and Erba 2015) documented at supra-regional scale (Tremolada et al. 2005, Visentin et al. 2021). It is characterized by the drastic reduction in abundance of schizosphaerellids that begins just stratigraphically preceding the negative CIE of the T-OAE and represents the wide-scale temporary collapse of a rock-forming taxon within the calcareous nannoplankton (Claps et al. 1995, Erba 2004, Tremolada et al. 2005, Mattioli et al. 2008, Fraguas et al. 2012, Hermoso et al. 2012, Erba et al. 2019a, Reolid et al. 2020, Visentin et al. 2021). In the Lombardy Basin, the "*Schizospaherella* crisis" is paralleled by a substantial decrease in abundance of another well-calcified nannofloral taxon, namely *Mitrolithus jansae* (Casellato and Erba 2015, Visentin and Erba 2021). In the negative CIE interval of the T-OAE *Schizosphaerella* is also characterized by reduced sizes (Mattioli and Pittet 2002, Mattioli et al. 2004, Mattioli et al. 2009, Suan et al. 2008, Suan et al. 2010, Reolid et al. 2014, Reolid et al. 2020, Clémence et al. 2015, Erba et al. 2019). These drastic reductions in calcareous nannoplankton calcification, also described as a 'calcareous nannofossil crisis' or 'disappearance event' (Bucefalo Palliani et al. 2002, Mattioli et al. 2004, Mattioli et al. 2008, Suan et al. 2008, Fraguas et al. 2012, Clémence et al. 2015), were translated into the drop in pelagic carbonate sedimentation as a consequence of combined warming, ocean fertilization and acidification influencing calcareous phytoplankton abundance and species-specific biocalcification. The increase in calcium carbonate above the Fish Level in both the Sogno and Gajum Cores (Figs. 2 and 3) records the resumption of *Schizosphaerella* production (Casellato and Erba 2015, Erba et al. 2019a, Visentin and Erba 2021), further highlighting the rock-forming role of this highly calcified taxon.

Jenkyns and Clayton (1986) observed a near-linear relationship (R^2 = 0.94) between carbon isotopes in organic matter and the calcium-carbonate content of the Fish Level formerly cropping out at Monte Brughetto. They interpreted this relationship as the result of the replacement of calcareous nannofossils by non-carbonate-secreting phytoplankton that preferentially fixed ^{12}C. However, the new data from the Sogno and Gajum Cores do not display such a linear relationship (Fig. 6). In fact, R^2 is equal to 0.006 and 0.002 for the Fish Level interval at Sogno and Gajum, respectively and a R^2 for the entire dataset equal to 0.26 and 0.10 at Sogno and Gajum, respectively. Furthermore, micropaleontological characterization of the Fish Level in the Colle di Sogno section (Casellato and Erba 2015), as well as in the Sogno and Gajum Cores (Visentin and Erba 2021), demonstrated that calcareous nannofossils

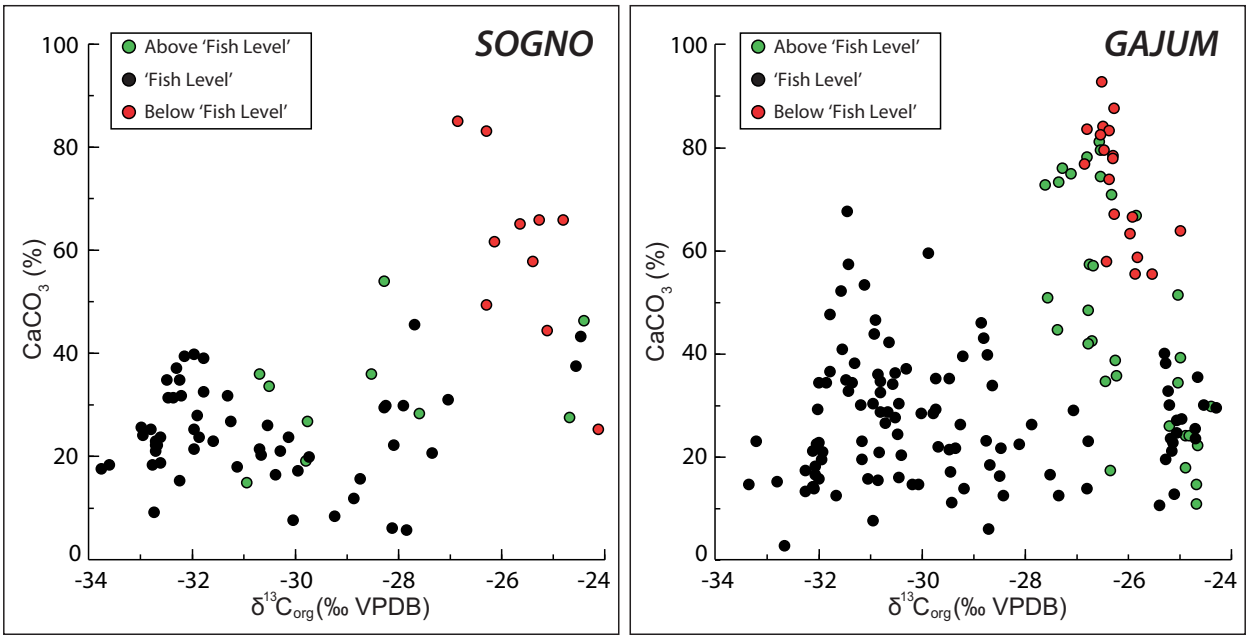

Fig. 6. Cross-plot of $CaCO_3$ versus $\delta^{13}C_{org}$ data for the Sogno and Gajum Cores. Samples below, within and above the Fish Level are indicated in red, black and green, respectively.

are present throughout the Fish Level, as in the intervals below and above. Consequently, the T-OAE negative excursion cannot be ascribed to a change in the nature and isotopic composition of the planktonic components due to local upwelling conditions, as hypothesized by Jenkyns and Clayton (1986). Moreover, the negative CIE has been documented in all complete marine and terrestrial archives, indicating that the whole ocean-atmosphere system was affected by a major change in the carbon pool.

The upper part of the grey interval within the Fish Level is characterized in both cores by a progressive increase in TOC up to ~1.4 %, with an average calcium carbonate content of 20–28 %. In both cores, the upper black interval displays the highest TOC content (up to ~2.5 %) associated with low $CaCO_3$ content (~27 %) (Unit 5 and Unit 4 in the Sogno and Gajum Cores, respectively). However, it should be noticed that in the Gajum Core a sharp decrease in TOC down to values of about 0.3 % was recognized in the very uppermost part of the Fish Level.

Possible dilution effects of organic matter by calcium carbonate were estimated by comparing measured TOC values with $CaCO_3$ content. In particular, TOC on a carbonate-free basis (TOC_{CF}) was calculated for both cores, in order to compensate for variable calcium carbonate amounts. TOC_{CF} curves do not show substantial variations with respect to TOC profiles, thus indicating a negligible impact of carbonate dilution on organic-matter content. This result is further confirmed by the lack of a direct correlation between TOC and $CaCO_3$, as shown in the cross-plot in Figure 7.

5.2. The carbon-isotope record in the Sogno and Gajum Cores

The $\delta^{13}C$ record of the latest Pliensbachian–early Toarcian time interval in both cores is characterized by common trends that ensure high-resolution dating and correlation between the two (Figs. 2 and 3). As described in section 4.1, the negative excursion in the Gajum Core is also marked by three lithostratigraphic intervals with particularly low $\delta^{13}C_{carb}$ values, from about –9 ‰ to about –12 ‰. Such punctuated very negative values (from –1 ‰ to –4 ‰) are also noted in the lower and middle part of the CIE of the Sogno Core (Fig. 2).

Although the overall trends in both carbonate and organic-carbon isotopes are similar in the Sogno and Gajum Cores, some differences exist in the $\delta^{13}C_{carb}$ absolute values of the two cores. In fact, the $\delta^{13}C_{org}$ values are practically identical, with the T-OAE chemostratigraphic anomaly represented by a negative

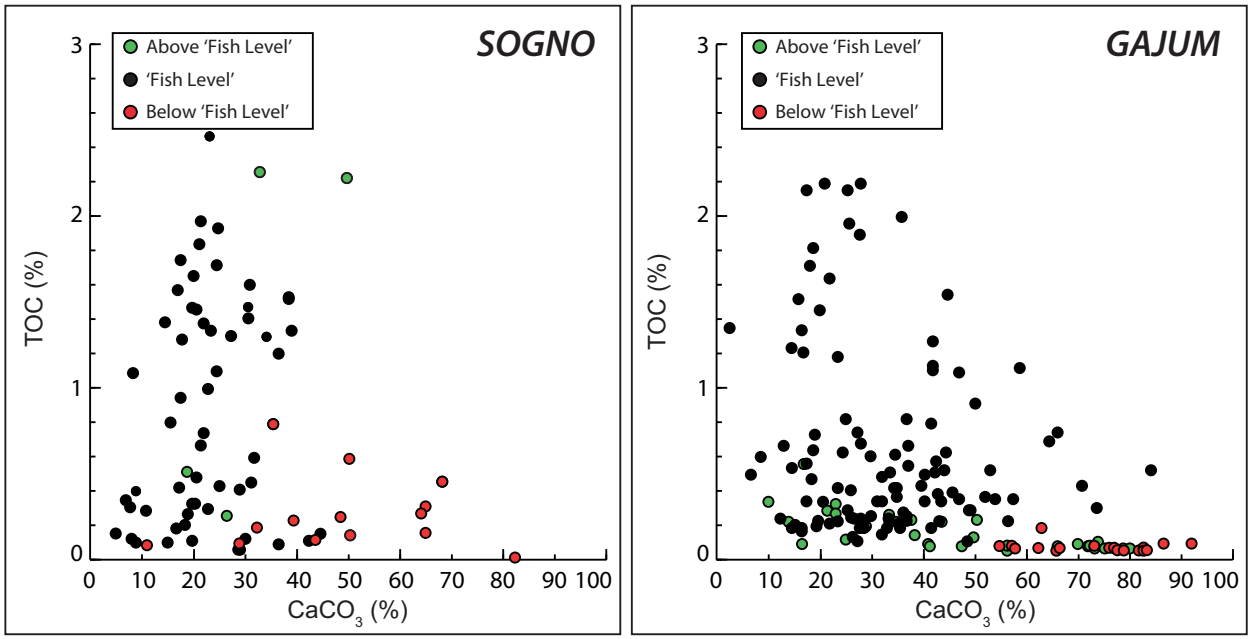

Fig. 7. Cross-plot of total organic carbon (TOC) versus $CaCO_3$ data for the Sogno and Gajum Cores. Samples below, within and above the Fish Level are indicated in red, black and green, respectively.

excursion of about 7 ‰ (Figs. 2 and 3). On the contrary, $\delta^{13}C_{carb}$ records of the two cores exhibit different values, with the amplitude of the T-OAE negative excursion reaching ~3 ‰ (from about 3 ‰ to about 0 ‰) in the Sogno Core, while this decrease is about twice as large (from about 3 ‰ to about –3 ‰) in the Gajum Core (Figs. 2 and 3). We speculate that these extremely negative values are related to the remineralization of organic matter and the fixation of relatively isotopically light carbon released below the sediment-water interface into authigenic carbonates. The preferential fixation of the released light carbon in the carbonate phase is illustrated by the occurrence of the very negative values exclusively in the carbonate-carbon but not in the organic-carbon isotopic record. Observed differences in the two $\delta^{13}C_{carb}$ records testify to the occurrence of variable early diagenetic patterns that acted to a different extent in the two locations.

An extensive discussion on the role of diagenesis was given by Jenkyns and Clayton (1986) to explain the low $\delta^{13}C$ values measured from several T-OAE organic-rich shales and intercalated manganoan carbonate from the Tethyan region, including the Monte Brughetto outcrop. They described the shift to lower values as the result of a negative local diagenetic trend unrelated to a change in the oceanic carbon-isotope reservoir. In particular, according to these authors, the negative values reflect a mixture of isotopically heavier primary marine carbonate and isotopically lighter diagenetic cement precipitated in equilibrium with CO_2 derived from bacterial oxidation of organic matter. The same interpretation was also given by Bellanca et al. (1999) to explain the low $\delta^{13}C_{carb}$ values in the lower Toarcian bioturbated manganoan limestones, grey marlstones, and thinly laminated, organic-carbon-rich black shales in the Belluno Basin (northeastern Italy) (Figs. 1E and 1F). Sabatino et al. (2011) described very negative $\delta^{13}C_{carb}$ values from manganoan and siliceous limestone interbedded within the T-OAE black-shale interval in the Julian Alps (Monte Mangart section). The authors suggested that the negative C-isotopic values coincident with high Mn contents indicate the effects of organic matter in the mineralization process during early diagenetic precipitation of manganese carbonates; the same interpretation is adopted here. As far as the Gajum Core is concerned, two of the three most negative $\delta^{13}C_{carb}$ intervals correlate with reddish limy cherts within Unit 5 (Figs. 2 and 3). Although the $\delta^{13}C_{carb}/\delta^{18}O_{carb}$ cross-plot (see below) is comparable with negligible diagenetic alteration, we cannot exclude the likely role of diagenesis due to the development of the limy cherts whose genesis necessarily involved dissolution–precipitation phenomena.

5.3. Oxygen-isotope variations

A cross-plot of $\delta^{13}C_{carb}$ values against the $\delta^{18}O_{carb}$ data for all the analysed samples of the two sections is given in Figure 8. A correlation between the two isotopic ratios is generally observed in samples affected by diagenesis due to the presence of variable quantities of isotopically homogeneous, isotopically negative calcite cementing primary marine carbonate (e. g., Marshall 1992, Blanchet et al. 2012). Our data show absence of correlation (R^2 equal to 0.21 and 0.07 in the Sogno and Gajum Cores, respectively) when considering all the analysed samples together. By grouping data according to their position relative to the Fish Level, no correlation between the $\delta^{13}C_{carb}$ and the $\delta^{18}O_{carb}$ is observed (R^2 from 0 to 0.19), with the exception of the interval above the Fish Level in the Gajum Core (R^2 = 0.56). These data suggest that diagenesis may have had little effect, with moderate impact only in the upper interval of the Gajum Core. Thus, the occurrence of common patterns in the oxygen-isotope record in the two sections suggests a relatively modest overprint of the original isotopic signal.

Some cautious considerations in terms of relative temperature variations can therefore be made. In both sections, a progressive shift of $\delta^{18}O_{carb}$ from heavier to lighter values is observed in correspondence with the Fish Level, possibly due to a gradual change towards warmer conditions. By considering the typical $\Delta^{18}O_{carb}$ gradients between 0.2–0.3 ‰ per °C for marine carbonates (Leng and Marshall 2004, Maslin and Dickson 2015), the observed $\delta^{18}O_{carb}$ decrease of about 2 ‰ in amplitude in both the Sogno and Gajum Cores would imply a warming of about 7–10 °C. This magnitude of warming is in good agreement with TEX_{86} based sea-surface temperatures reconstructions for the Tethyan region for the same time interval (Ruebsam et al. 2020).

In the Sogno Core, where the lowermost part of the Sogno Formation is preserved, the progressive shift in $\delta^{18}O_{carb}$ towards lower values begins before the deposition of the Fish Level, suggesting that the onset of warmer conditions pre-dated the deposition of the black-shale interval. In fact, oxygen-isotope values start to gently decrease from about 3 metres below the Fish Level and then are marked by a sharp shift to lighter ratios at the onset level of the negative carbon-isotope anomaly, about 0.5 m below the base of the black-shale interval. Oxygen-isotope values in the uppermost part of the succession record a progressive shift back to higher values, probably resulting from a gradual cooling. In the Gajum Core, the abrupt shift to lighter $\delta^{18}O_{carb}$ values coincides with the base of the Fish Level and is consistent with the occurrence of a hiatus at the Domaro Limestone/Sogno Formation boundary. The most negative values are reached in the uppermost part of the black-shale interval (from about 16.2 to 12.8 m) followed by a gradual increase. We note particularly that, in both cores, the gradual shift back to higher oxygen-isotope ratios occurs prior to the end of the negative carbon-isotope anomaly,

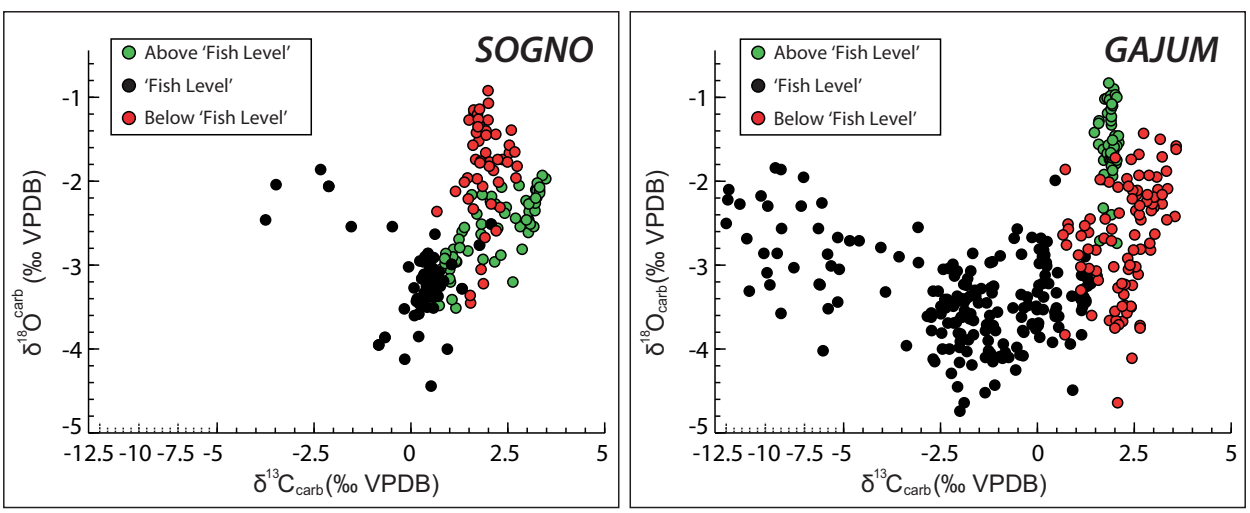

Fig. 8. Cross-plot of $\delta^{18}O_{carb}$ versus $\delta^{13}C_{carb}$ data for the Sogno and Gajum Cores. Samples below, within and above the Fish Level are indicated in red, black and green, respectively. For the sake of readability, lower $\delta^{13}C_{carb}$ values are reported using a different scale.

indicating that the transition towards cooler conditions started before the return back to post-T-OAE $\delta^{13}C$ background values. Indeed, it should be pointed out that local variations in salinity might have influenced the observed $\delta^{18}O_{carb}$ record, in addition to temperature. However, such effects cannot be constrained with available data.

The lowest $\delta^{18}O_{carb}$ values measured in the upper part of the negative $\delta^{13}C$ anomaly in both the Sogno and Gajum Cores are consistent with other Tethyan sequences observed in Spain (Tremolada et al. 2005, Gómez et al. 2016), Portugal (Oliveira et al. 2006, Suan et al. 2008), Greece (Kafousia et al. 2014), and north European localities in France (Emmanuel et al. 2006) and Germany (Röhl et al. 2001).

5.4. The T-OAE in the western Tethys

Recently, Hougård et al. (2021) documented the T-OAE anomalies in the Swabo-Franconian Basin (SW Germany) and discussed the extension of anoxia relative to carbon-isotope chemostratigraphy. Results were compared to similar datasets from the Paris Basin, the Cleveland Basin and the Swiss Jura to assess synchroneity/diachroneity of the termination of anoxia in different parts of the seaway connecting the Tethys to the Boreal Oceans. Hougård et al. (2021) raised the critical issue of the definition of the T-OAE that hitherto has not been systematically applied, thereby introducing artefacts and/or misunderstandings in correlations and modelling at supra-regional scale.

Following the original definition of OAEs by Schlanger and Jenkyns (1976), Jenkyns (1988) described the lithological T-OAE signature based on globally distributed apparently coeval organic-rich black shales dated to the early Toarcian *falciferum* Zone. This lithostratigraphy-based definition was applied in several subsequent papers and complemented by a broad $\delta^{13}C$ positive excursion interrupted by an abrupt negative "bite" in its central portion (Jenkyns 2010). In Figure 9, the $\delta^{13}C$ reference curve for the latest Pliensbachian–middle Toarcian time interval (Ruebsam and Al-Husseine 2020, modified by Hougård et al. 2021), shows the prolonged positive excursion containing the negative CIE. The extremely detailed record of the Mochras borehole (Xu et al. 2018, Storm et al. 2020) documents the T-OAE positive excursion (from the mid-*tenuicostatum* Zone to the mid-*serpentinum* Zone) and the negative CIE (*exaratum* Subzone). Applying the GTS2020 time scale (Gradstein et al. 2020) the broad positive carbon-isotope excursion corresponds to a ~1.5 million-year-long interval. The remarkable $\delta^{13}C$ negative CIE has been documented at global scale in a variety of marine and continental settings indicating a global perturbation of the C cycle (see reviews by Remirez and Algeo 2020, Ruebsam and Al-Husseini 2020). Arguably, such a negative CIE is the most consistently recognizable feature that accompanies the T-OAE.

Müller et al. (2017) proposed renaming the T-OAE as the Jenkyns Event in which they distinguished the negative CIE (their interval 2). Recently, Reolid et al. (2020) recommended using the term Jenkyns Event for the global early Toarcian changes including anoxia, enhanced organic-matter burial, biotic crises in marine and terrestrial ecosystems, warming and sea-level rise. However, a precise definition of the beginning and end of the Jenkyns Event is not provided, hampering its unambiguous identification and correlation on a regional, supra-regional and global scale.

Here, we suggest labelling as the Jenkyns Event only the $\delta^{13}C$ negative CIE of the T-OAE. As such, the Jenkyns Event correlates with the uppermost *tenuicostatum* Zone–*exaratum* Subzone and falls within the NJT6 nannofossil Zone (Ferreira et al. 2019, Visentin and Erba 2021). Inspection of medium- to high-resolution records allows a further subdivision of the Jenkyns Event into: a) a lower part where, after a marked decrease, the carbon-isotope curve remains at minimum values, and b) an upper part that features a gradual increase back to pre-anomaly values (Fig. 9). It is worth pointing out that the chemostratigraphic expression of the lower part of the Jenkyns Event (J1) can have very different shapes, while the upper part (J2) is similar in the currently available documented records. Adopting the above subdivision, three time-lines can be used for global correlations, namely the base of J1, the base of J2, and the top of J2.

The comparison of lithostratigraphy and chemostratigraphy (both $\delta^{13}C_{carb}$ and $\delta^{13}C_{org}$ data) highlights analogies and differences in the timing and depositional style of the Fish Level in the Sogno and Gajum Cores (Fig. 9). At both sites, the lowermost part of the lithostratigraphically constrained T-OAE (Fish Level) corresponds to carbonate- and TOC-poor marlstones and marly claystones, followed in the middle and upper parts by more organic-rich dark grey marly claystones and black shales. The coherence in stratigraphic position of the TOC content in the two cores seems to imply some remineralization of organic matter (hence lower TOC) in the early stages of the Jenkyns Event (lower

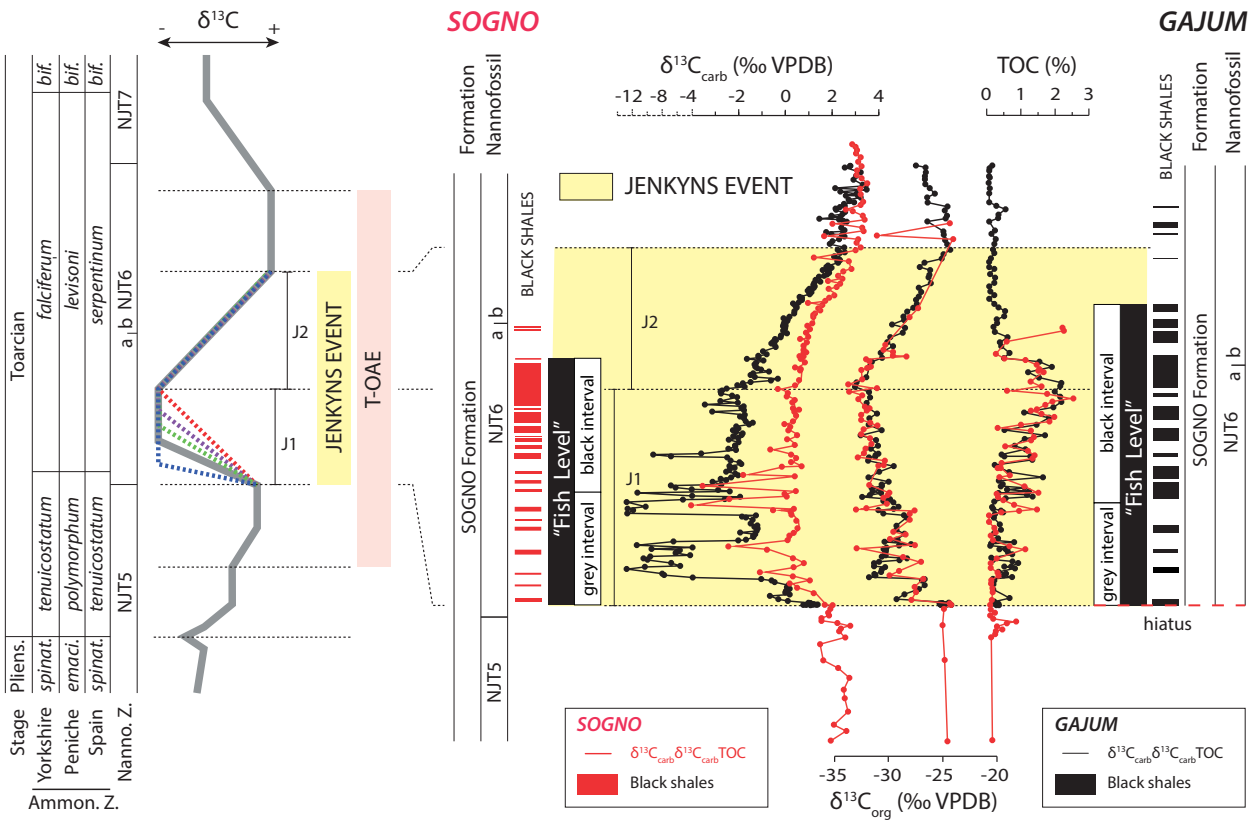

Fig. 9. On the left, the schematic $\delta^{13}C$ reference curve for the latest Pliensbachian–Toarcian time interval is reported (modified after Ruebsam and Al-Husseini (2020), with minor modifications by Hougård et al. 2021). The stratigraphic extent of the T-OAE is indicated with a light red rectangle, while the proposed interval of the Jenkyns Event is indicated by a yellow band. Extent of the lower J1 and the upper J2 segments of the Jenkyns Event is also illustrated. Coloured dashed lines in the reference plot represent the different trends documented in the lower part of the Jenkyns Event (J1). On the right, chemostratigraphic correlation of the Sogno and Gajum Cores is based on overlapped $\delta^{13}C_{carb}$ and $\delta^{13}C_{org}$ isotope profiles and TOC data. The extent of the Fish Level and its internal subdivision into a grey interval and a black interval is reported for the two records.

half of the J1) that could have fuelled authigenic carbonate precipitation after burial.

In both the Sogno and Gajum Cores, the base of the Fish Level coincides with the chemostratigraphic onset of the Jenkyns Event (Figs. 2, 3, and 9). This correlation implies that the hiatus at the Domaro Limestone/Sogno Formation boundary in the Gajum Core does not cut out the basal part of the Fish Level. We underscore the fact that, in the Sogno Core, decreases in $CaCO_3$ and $\delta^{18}O$ start ~20 cm below the base level of the signature of the Jenkyns Event, in a similar way to records from the Sancerre section (Hermoso et al. 2013). In the Gajum Core, the coeval interval seems either extremely condensed or absent/elided.

The timing of initial deposition of the Fish Level relative to the CIE is synchronous at both Sogno and Gajum sites. Conversely, the upper boundary of the black-shale interval appears diachronous in the two records (Fig. 9) suggesting a delayed re-establishment of well-oxygenated conditions at Gajum. Moreover, the top of the black-shale interval is abrupt at Sogno, whereas a gradual change from black shales to organic-lean pale marlstones is documented in the Gajum Core (Figs. 2, 3 and 4). This observed disparity is interpreted to reflect the different geological settings: on a pelagic plateau at about 1500 m water depth (Sogno Core) and in an inner basin along the slope of a structural high at about 1000 m water depth (Gajum Core). Therefore, the lithostratigraphic expression of the T-OAE, namely the Fish Level, was of similar inception, but different termination and duration depending on local conditions even within the same basin.

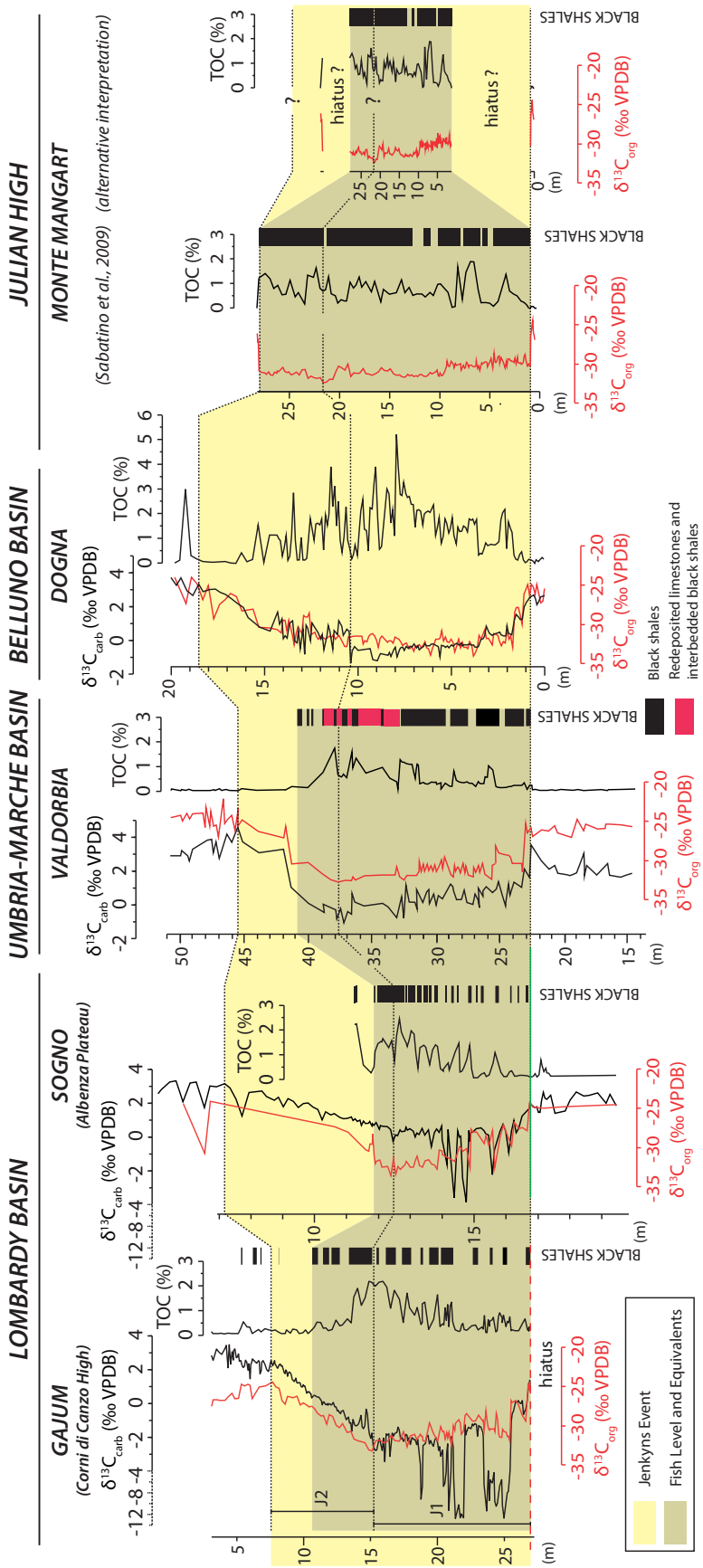

Fig. 10. Correlation of carbon-isotope profiles ($\delta^{13}C_{carb}$ in black and $\delta^{13}C_{org}$ in red), TOC and black-shale occurrence for the Jenkyns Event interval at Sogno (Lombardy Basin, this study), Gajum (Lombardy Basin, this study), Valdorbia (Umbria-Marche Basin, Sabatino et al. 2009), Dogna (Belluno Basin, Jenkyns et al. 2001, Sabatino et al. 2009), and the Monte Mangart section (Julian High, Sabatino et al. 2009, Sabatino et al. 2011). An alternative interpretation of the Monte Mangart data is also reported. See text for details. The stratigraphic position of the Fish Level and Fish Level Equivalent is indicated by a grey band, while the position of the Jenkyns Event interval is highlighted by a yellow band.

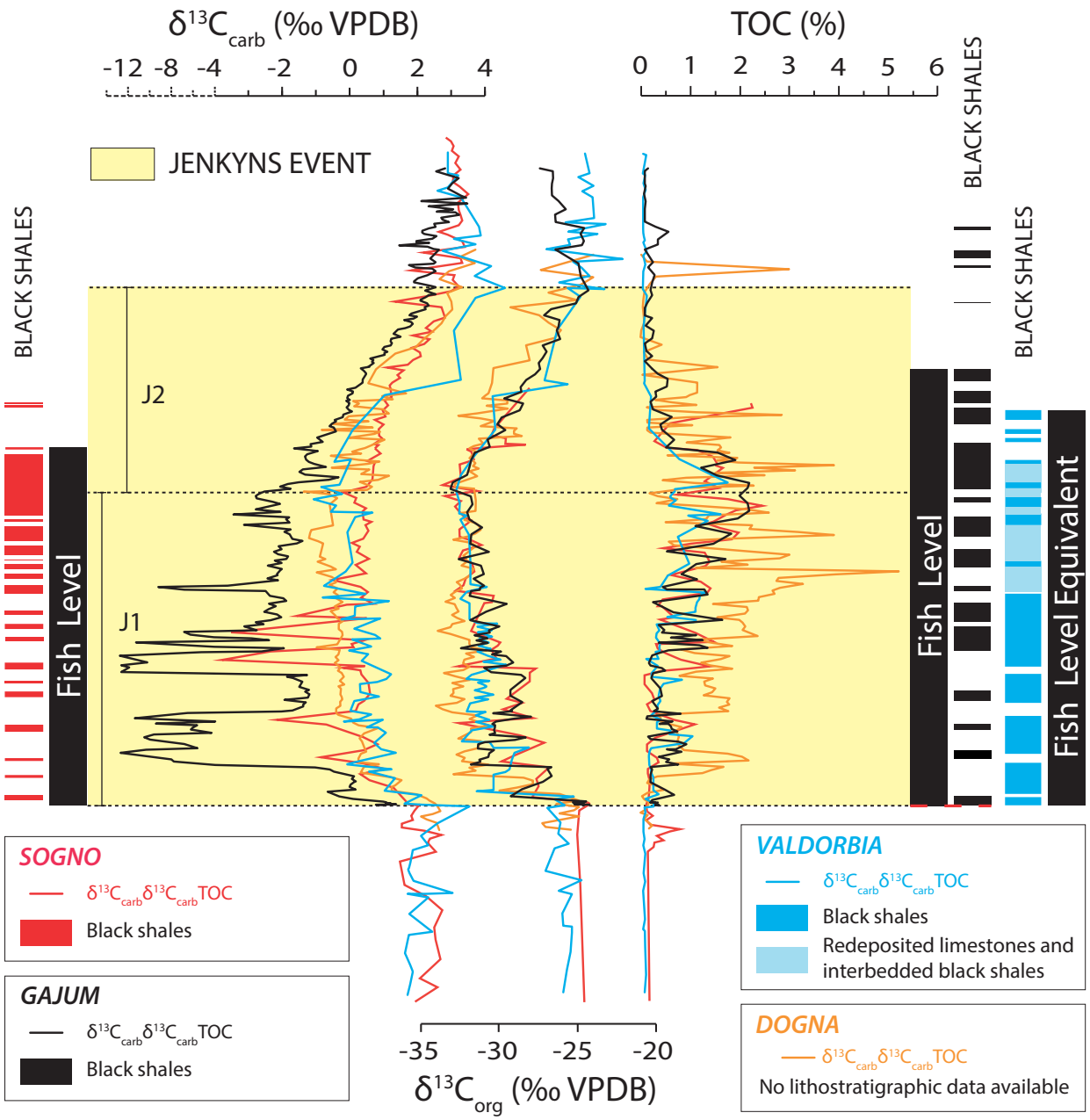

Fig. 11. Overlain $\delta^{13}C_{carb}$, $\delta^{13}C_{org}$, and TOC profiles for the Sogno Core (Lombardy Basin, this study), Gajum Core (Lombardy Basin, this study), Valdorbia (Umbria-Marche Basin, Sabatino et al. 2009), Dogna (Belluno Basin, Jenkyns et al. 2001, Sabatino et al. 2009). The distribution of the black-shale intervals (Fish Level and Fish Level Equivalent) is also reported.

In Figure 10 the Sogno and Gajum C-isotopic, black-shale and TOC records are compared to analogous data from the Umbria-Marche Basin (Valdorbia section, Sabatino et al. 2009), Belluno Basin (Dogna section; in Jenkyns et al. 2001, Sabatino et al. 2009) and Julian High (Monte Mangart section in Sabatino et al. 2009, Sabatino et al. 2011). The negative CIE at Valdorbia and Dogna unambiguously allows the identification and correlation of the J1 and J2 segments at supra-regional scale. The $\delta^{13}C_{org}$ record of the Monte Mangart section was interpreted as complete, allowing the identification of the base and top of the negative CIE (Sabatino et al. 2009). However, based on values and trends, we propose a revised chemostratigraphic cor-

relation suggesting that hiatuses have removed the oldest and youngest parts of the record of the Jenkyns Event (Fig. 10).

From a lithostratigraphic point of view, a Fish Level Equivalent is recognizable in the Valdorbia and Monte Mangart sections, whereas lithological data are not provided for Dogna, preventing the identification of a Fish Level Equivalent in the Belluno Basin. Chemostratigraphy indicates that the Fish Level Equivalent corresponds to the entire J1 and lower J2 in the Umbria-Marche Basin, similarly to the Lombardy Basin (Fig. 11). While the base of the Fish Level Equivalent is synchronous to the base of the Fish Level, in the Umbria-Marche Basin (Valdorbia section) the termination of anoxia (= top of the Fish Level Equivalent) is younger than at Sogno and older than at Gajum (Figs. 10 and 11). Depending on the interpretation of the carbon-isotope record, at Monte Mangart the Fish Level Equivalent might coincide with the entire Jenkyns Event interval following the interpretation of Sabatino et al. (2009). Thus, the base of the Fish Level Equivalent would be synchronous with the records in the Lombardy and Umbria-Marche Basins while the top would be delayed for at least one locality on the Julian High (Monte Mangart). The revised chemostratigraphy (this study), implying stratigraphic gaps at the base and top of the Fish Level Equivalent, hampers the assessment of synchroneity/diachroneity of inception and/or termination of oxygen depletion in the Julian High area.

As far as the TOC is concerned (Figs. 10 and 11), the Valdorbia and Dogna records are similar to those of Sogno and Gajum, with an increase from the beginning of the negative CIE to the J1/J2 boundary interval. However, whereas at Valdorbia the TOC values are comparable to the Sogno and Gajum data, values are higher at Dogna (from 0.3 to 5 %). Moreover, in the Dogna section, the increase in TOC begins lower in the section and terminates higher than at Sogno, Gajum and Valdorbia.

At supra-regional scale within the western Tethys litho-geochemical data indicate that features were very similar in the Lombardy and Umbria-Marche Basins, but slightly different in the Belluno Basin. The onset of black-shale deposition (Fish Level and Fish Level Equivalent) was coeval at inter-basinal scale since it coincides with the beginning of the Jenkyns Event in the Lombardy and Umbria-Marche Basins. Termination of black-shale deposition, however, was diachronous at intra- and inter-basinal scale, possibly depending on specific morphostructural settings.

6. Conclusions

New carbon- and oxygen-isotope, $CaCO_3$ and TOC data from the Sogno and Gajum Cores provide a high-resolution record of the T-OAE in the Lombardy Basin. The reconstructed palaeobathymetry is about 1000 and 1500 m water depth for the Gajum and Sogno sites, respectively. Thus, the investigated sections provide some of the deepest records of the T-OAE in the western Tethyan region. During the early Toarcian, sedimentation shifted to a depositional style characterized by dark grey to black marly claystones with low $CaCO_3$, corresponding to the Fish Level. This interval is lithologically variable and of significantly different thickness in the Sogno (~5 m) and Gajum (~16 m) Cores. Notwithstanding these differences, in both cores the Fish Level is marked by a lower part characterized by minimum $CaCO_3$ (5–10 %) and TOC (~0.2 %), a central part with a progressive shift in TOC up to ~1.4 %, and an upper part with the highest TOC values reaching up to ~2.5 %. Based on detailed lithostratigraphy, the Fish Level is subdivided into a lower grey interval and an upper black interval, the latter being the Fish Level *sensu stricto*.

In the Sogno Core, the carbon-isotope chemostratigraphy allows the identification of the minor negative anomaly at the Pliensbachian/Toarcian boundary followed by a broad positive excursion. A hiatus elides the lowermost part of the Sogno Formation below the Fish Level in the Gajum Core, so that the Pliensbachian/Toarcian boundary interval is not preserved. Across the Fish Level, the negative carbonate carbon-isotope anomaly shows a shift of ~3 ‰ in the Sogno and ~6 ‰ in the Gajum Core, respectively, and a $\delta^{13}C_{org}$ negative shift of ~7 ‰ in both successions. We propose naming the $\delta^{13}C$ negative anomaly the 'Jenkyns Event' (further subdivided into the J1 and J2 segments) and use this diagnostic geochemical feature to unambiguously identify the T-OAE at a global scale. Calcareous nannofossil biostratigraphy constrains the Jenkyns Event to the NJT 6 Zone.

In both cores, oxygen-isotope data document a progressive shift to lighter values suggestive of warmer conditions starting before the deposition of the Fish Level. The lowest oxygen-isotope ratios are recorded within the Fish Level itself, consistent with warmest ocean temperatures during its deposition in the early Toarcian. Data indicate a return back to higher oxygen-isotope values before the end of the black-shale deposition, thus suggesting that a change to cooler conditions occurred before the termination of the Jenkyns Event.

High-resolution correlation of the new cored sequences from the Lombardy Basin highlights the fact that the onset of deposition of the Fish Level was synchronous, but its termination was diachronous at the two sites, suggesting a delayed re-establishment of oxygenated bottom-water conditions at Gajum. Also, the top of the black-shale interval is abrupt at Sogno, whereas black shales gradually change to grey marlstones in the Gajum Core.

The records from the Lombardy Basin can be compared to sections from the Umbria-Marche and Belluno Basins and the Julian High with the $\delta^{13}C_{carb}$ and $\delta^{13}C_{org}$ data providing the chemostratigraphic framework (J1 and J2 segments) to assess the wider distribution of TOC and black shales. As is the case for other OAEs (see discussion in Tsikos et al. 2004 and Kolonic et al. 2005 for OAE2, and Wagner et al. 2013 for OAE3), the organic-rich and/or carbonate-poor lithologies (black shales) are diachronous relative to carbon-isotope stratigraphy. Specifically, the onset of the T-OAE black shale deposition in the western Tethys was coeval in different basins and started at the beginning of the Jenkyns Event, but the return to more oxygenated bottom waters was diachronous at local to inter-basinal scales.

Acknowledgements. The authors are grateful to Guillaume Suan and an anonymous Reviewer who, with their valuable comments, greatly contributed to improving the quality of the manuscript. We thank C. Compostella, E. S. Ferrari and M. Pegoraro (University of Milano) and S. Nicoara (Open University) for their technical help. The research was conducted within the PRIN 2017RX9XXXY awarded to EE and the Italian Ministry of Education (MIUR) project "Dipartimenti di Eccellenza 2018–2022, Le Geoscienze per la Società: Risorse e loro evoluzione".

References

Al-Suwaidi, A. H., Angelozzi, G. N., Baudin, F., Damborenea, S. E., Hesselbo, S. P., Jenkyns, H. C., Manceñido, M. O., Riccardi, A. C., 2010. First record of the Early Toarcian Oceanic Anoxic Event from the Southern Hemisphere, Neuquén Basin, Argentina. Journal of the Geological Society of London 167, 633–636.

Bellanca, A., Masetti, D., Neri, R., Venezia, F., 1999. Geochemical and sedimentological evidence of productivity cycles recorded in Toarcian black shales from the Belluno Basin, Southern Alps, Northern Italy. Journal of Sedimentary Research 69, 466–476.

Bernoulli, D., Homewood, P., Kälin, O., van Stuijvenberg, J., 1979. Evolution of continental margins in the Alps. Schweizerische Mineralogische und Petrographische Mitteilungen 59, 165–170.

Bernoulli, D., Jenkyns, H. C., 1974. Alpine, Mediterranean, and Central Atlantic Mesozoic facies in relation to the early evolution of the Tethys. In: Dott, R. H., Shaver, R. H. (Eds.), Modern and Ancient Geosynclinal Sedimentation. Society of Economic Paleontologists and Mineralogists, Special Publication 19, 129–160.

Bernoulli, D., Jenkyns, H. C., 2009. Ancient oceans and continental margins of the Alpine-Mediterranean Tethys: Deciphering clues from Mesozoic pelagic sediments and ophiolites. Sedimentology 56, 149–190.

Bjerrum, C. J., Surlyk, F., Callomon, J. H., Slingerland, R. L., 2001. Numerical paleoceanographic study of the Early Jurassic transcontinental Laurasian Seaway. Paleoceanography 16, 390–404.

Blanchet, C. L., Kasten, S., Vidal, L., Poulton, S. W., Ganeshram, R., Thouveny, N., 2012. Influence of diagenesis on the stable isotopic composition of biogenic carbonates from the Gulf of Tehuantepec oxygen minimum zone. Geochememistry, Geophysics, Geosystems 13, Q04003, doi: 10.1029/2011GC003800.

Bosellini, A., Winterer, E. L., 1975. Pelagic limestone and radiolarite of the Tethyan Mesozoic: a genetic model. Geology 3, 279–282.

Bosence, D., Procter, E., Aurell, M., Kahla, A. B., Boudagher-Fadel, M., Casaglia, F., Cirilli, S., Mehdie, M., Nieto, L., Rey, J., Scherreiks, R., Soussi, M., Waltham, D., 2009. A Dominant Tectonic Signal in High-Frequency, Peritidal Carbonate Cycles? A Regional Analysis of Liassic Platforms from Western Tethys. Journal of Sedimentary Research 79, 389–415.

Bucefalo Palliani, R., Mattioli, E., Riding, J. B., 2002. The response of marine phytoplankton and sedimentary organic matter to the Early Toarcian (Lower Jurassic) oceanic anoxic event in northern England. Marine Micropaleontology 46, 223–245.

Caruthers, A. H., Gröcke, D. R., Smith, P. L., 2011. The significance of an Early Jurassic (Toarcian) carbon-isotope excursion in Haida Gwaii (Queen Charlotte Islands), British Columbia, Canada. Earth and Planetary Science Letters 307, 19–26.

Casellato, C. E., Erba, E., 2015. Calcareous nannofossil biostratigraphy and paleoceanography of the Toarcian Oceanic Anoxic Event at Colle di Sogno section (Southern Alps, Italy). Rivista Italiana di Paleontologia e Stratigrafia 105, 343–376.

Castellarin, A., 1972. Evoluzione paleotettonica sinsedimentaria del limite tra 'Piattaforma Veneta' e 'Bacino Lombardo', a nord di Riva del Garda. Giornale di Geologia, serie 2a 38, 11–212.

Channell, J. E. T., Casellato, C. E., Muttoni, G., Erba, E., 2010. Magnetostratigraphy, nannofossil stratigraphy and apparent polar wander for Adria-Africa in the Jurassic–Cretaceous boundary interval. Palaeogeography, Palaeoclimatology, Palaeoecology 293, 51–75.

Claps, M., Erba, E., Masetti, D., Melchiorri, F., 1995. Milankovitch-type cycles recorded in Toarcian black

shales from Belluno Trough (Southern Alps, Italy). Memorie di Scienze Geologiche, Università di Padova 47, 179–188.

Clémence, M. E., Gardin, S., Bartolini, A., 2015. New insights in the pattern and timing of the Early Jurassic calcareous nannofossil crisis. Paleogeography, Paleoclimatology, Paleoecology 427, 100–108.

Cohen, A. S., Coe, A. L., Harding, S. M., Schwark, L., 2004. Osmium isotope evidence for the regulation of atmospheric CO_2 by continental weathering. Geology 32, 157–160.

Coplen, T. B., 1994. Reporting of stable hydrogen, carbon, and oxygen isotopic abundances. Pure and Applied Chemistry 66, 273–276.

da Rocha, R. B., Mattioli, E., Duarte, L. V., Pittet, B., Elmi, S., Mouterde, R., Cabral, M. C., Comas-Rengifo, M. J., Gómez, J. J., Goy, A., Hesselbo, S. P., Jenkyns, H. C., Littler, K., Mailliot, S., de Oliveira, L. C. V., Osete, M. L., Perilli, N., Pinto, S., Ruget, C., Suan, G., 2016. Base of the Toarcian Stage of the Lower Jurassic defined by the Global Boundary Stratotype Section and Point (GSSP) at the Peniche section (Portugal). Episodes 39, 460–481.

Dera, G., Brigaud, B., Monna, F., Laffont, R., Pucéat, E., Deconinck, J.-F., Pellenard, P., Joachimski, M. M., Durlet, C., 2011. Climatic ups and downs in a disturbed Jurassic world. Geology 39, 215–218.

Emmanuel, L., Renard, M., Cubaynes, R., De Rafelis, M., Hermoso, M., Lecallonnec, L., Le Solleuz, A., Rey, J., 2006. The "Schistes Carton" of Quercy (Tarn, France): a lithological signature of a methane hydrate dissociation event in the early Toarcian. Implications for correlations between Boreal and Tethyan realms. Bulletin de la Société Géologique de France 177, 239–249.

Erba, E., 2004. Calcareous nannofossils and Mesozoic oceanic anoxic events. Marine Micropaleontology 52, 85–106.

Erba, E., Bottini, C., Faucher, G., Gambacorta, G., Visentin, S., 2019a. The response of calcareous nannoplankton to Oceanic Anoxic Events: The Italian pelagic record. Bollettino della Società Paleontologica Italiana 58, 51–71.

Erba, E., Casellato, C. E., 2010. Paleoceanografia del Giurassico nella Tetide occidentale: l'archivio geologico del Bacino Lombardo, Rendiconti dell'Istituto Lombardo. Accademia di Scienze e Lettere, Special Publication on "Una nuova Geologia per la Lombardia" 447, 115–140.

Erba, E., Gambacorta, G., Visentin, S., Cavalheiro, L., Reolon, D., Faucher, G., Pegoraro, M., 2019b. Coring the sedimentary expression of the early Toarcian Oceanic Anoxic Event: new stratigraphic records from the Tethys Ocean. Scientific Drilling 26, 17–27.

Ettinger, N. P., Larson, T. E., Kerans, C., Thibodeau, A. M., Hattori, K. E., Kacur, S. M., Martindale, R. C., 2021. Ocean acidification and photic-zone anoxia at the Toarcian Oceanic Anoxic Event: Insights from the Adriatic Carbonate Platform. Sedimentology 68, 63–107.

Fantasia, A., Föllmi, K. B., Adatte, T., Bernaìrdez, E., Spangenberg, J. E., Mattioli, E., 2018. The Toarcian Oceanic Anoxic Event in southwestern Gondwana: an example from the Andean Basin, northern Chile. Journal of the Geological Society 175, 883–902.

Fantasia, A., Föllmi, K. B., Adatte, T., Spangenberg, J. E., Mattioli, E., 2019. Expression of the Toarcian Oceanic Anoxic Event: New insights from a Swiss transect. Sedimentology 66, 262–284.

Ferreira, J., Mattioli, E., Sucheràs-Marx, B., Giraud, F., Duarte, V. L., Pittet, B., Suan, G., Hassler, A., Spangenberg, J. E., 2019. Western Tethys Early and Middle Jurassic calcareous nannofossil biostratigraphy. Earth-Science Reviews 197, 1–19.

Filatova, N. I., Konstantinovskaya, E., Vishnevskaya, V., 2020. Jurassic–Lower Cretaceous siliceous rocks and black shales from allochthonous complexes of the Koryak-Western Kamchatka orogenic belt, East Asia. International Geology Review, doi: 10.1080/00206814.2020.1848649.

Fraguas, A., Comas-Rengifo, M. J., Gómez, J., Goy, A., 2012. The calcareous nannofossil crisis in Northern Spain (Asturias province) linked to the Early Toarcian warming-driven mass extinction. Marine Micropaleontology 94–95, 58–71.

Frimmel, A., Oschmann, W., Schwark, L., 2004. Chemostratigraphy of the Posidonia Black Shale, SW Germany: I. Influence of sea-level variation on organic facies evolution. Chemical Geology 206, 199–230.

Gaetani, M., 1975. Jurassic stratigraphy of the Southern Alps: a review. In: Squyres, C. H. (Ed.), Geology of Italy, I, Earth Sciences Society of the Libyan Arab Republic, Tripoli, Libya, 377–402.

Gaetani, M., 2010. From Permian to Cretaceous: Adria as pivotal between extensions and rotations of Tethys and Atlantic Oceans. In: Beltrando, M., Peccerillo, A., Mattei, M., Conticelli, S., Doglioni, C. (Eds.), The Geology of Italy. Journal of the Virtual Explorer 36, paper 5.a, https://doi.org/10.3809/jvirtex.2010.00235, 2010.

Gaetani, M., Erba, E., 1990. Il Bacino Lombardo: un sistema paleoalto/fossa in un margine continentale passivo durante il Giurassico. 75° Congresso Società Geologica Italiana, 10–12 September 1990, Milano, Italy. Guida all'escursione A3.

Gaetani, M., Poliani, G., 1978. Il Toarciano e il Giurassico medio in Albenza (Bergamo). Rivista Italiana di Paleontologia e Stratigrafia 84, 349–382.

Gómez, J. J., Comas-Rengifo, M. J., Goy, A., 2016. Palaeoclimatic oscillations in the Pliensbachian (Early Jurassic) of the Asturian Basin (Northern Spain). Climate of the Past 12, 1199–1214.

Gradstein, F. M., Ogg, J. G., Schmitz, M. D., Ogg, G. M., 2020. Geological Time Scale 2020. Elsevier, 2 volumes, 1390 p.

Gröcke, D. R., Hori, R. S., Trabucho-Alexandre, J., Kemp, D. B., Schwark, L., 2011. An open ocean record of the Toarcian oceanic anoxic event. Solid Earth 2, 245–257.

Hallam, A., 1967. The depth significance of shales with bituminous laminae. Marine Geology 5, 481–493.

Hallam, A., 1981. A revised sea-level curve for the early Jurassic. Journal of the Geological Society 138, 735–743.

Haq, B. U., Hardenbol, J., Vail, P. R., 1987. Chronology of fluctuating sea-levels since the Triassic. Nature 235, 1156–1167.

Hardenbol, J., Thierry, J., Farley, M. B., Jacquin, T., de Graciansky, P.-C., Vail, P. R., 1998. Mesozoic and Cenozoic sequence chronostratigraphic framework of European basins. In: de Graciansky, P.-C., Hardenbol, J., Jacquin, T., Vail, P. R. (Eds.), Mesozoic and Cenozoic sequence stratigraphy of European basins. Society for Sedimentary Geology (SEPM), Special Publication 60, 3–13, charts 1–8, Tulsa, Oklahoma.

Heimdal, T. H., Goddéries, Y., Jones, M. T., Svensen, H. H., 2021. Assessing the importance of thermogenic degassing from the Karoo Large Igneous Province (LIP) in driving Toarcian carbon cycle perturbations. Nature Communications 12, doi: 10.1038/s41467-021-26467-6.

Hermoso, M., Minoletti, F., Pellenard, P., 2013. Black shale deposition during Toarcian super-greenhouse driven by sea level. Climate of the Past 9, 2703–2712.

Hermoso, M., Minoletti, F., Rickaby, R. E. M., Hesselbo, S. P., Baudin, F., Jenkyns, H. C., 2012. Dynamics of a stepped carbon-isotope excursion: Ultra high-resolution study of Early Toarcian environmental change. Earth and Planetary Science Letters 319–320, 45–54.

Hesselbo, S. P., Gröcke, D. R., Jenkyns, H. C., Bjerrum, C. J., Farrimond, P., Morgans Bell, H. S., Green, O. R., 2000. Massive dissociation of gas hydrate during a Jurassic Oceanic Anoxic Event. Nature 406, 392–395.

Hesselbo, S. P., Jenkyns, H. C., 1998. British Lower Jurassic sequence stratigraphy. In: de Graciansky, P. C., Hardenbol, J., Jacquin, T., Farley, M., Vail, P. R. (Eds.), Mesozoic–Cenozoic Sequence Stratigraphy of European Basins, Society for Sedimentary Geology (SEPM), Special Publication 60, 561–581.

Hesselbo, S. P., Jenkyns, H. C., Duarte, L. V., Oliveira, L. C. V., 2007. Carbon-isotope record of the Early Jurassic (Toarcian) Oceanic Anoxic Event from fossil wood and marine carbonate (Lusitanian Basin, Portugal). Earth and Planetary Science Letters 253, 455–470.

Hesselbo, S. P., Pieńkowski, G., 2011. Stepwise atmospheric carbon-isotope excursion during the Toarcian Oceanic AnoxicEvent (Early Jurassic, Polish Basin). Earth and Planetary Science Letters 301, 365–372.

Hinnov, L. A., Park, J., Erba, E., 2000. Lower–Middle Jurassic rhythmites from the Lombard Basin, Italy: a record of orbitally forced carbonate cycles modulated by secular environmental changes in West Tethys. In: Hall, R. L., Smith, P. L. (Eds.), Advances in Jurassic Research, Trans Tech Publications, Zürich, Switzerland, 437–454.

Hougård, I. W., Bojese-Koefoed, J. A., Vickers, M. L., Ullmann, C. V., Bjerrum, C. J., Rizzi, M., Korte, C., 2021. Redox element record shows that environmental perturbations associated with the T-OAE were of longer duration than the carbon isotope record suggests – the Aubach section, SW Germany. Newsletters on Stratigraphy 54, 229–246.

Ikeda, M., Hori, R. S., Ikehara, M., Miyashita, R., Chino, M., Yamada, K., 2018. Carbon cycle dynamics linked with Karoo-Ferrar volcanism and astronomical cycles during Pliensbachian-Toarcian (Early Jurassic). Global and planetary Change 170, 163–171.

Izumi, K., Kemp, D. B., Itamiya, S., Inui, M., 2018. Sedimentary evidence for enhanced hydrological cycling in response to rapid carbon release during the early Toarcian oceanic anoxic event. Earth and Planetary Science Letters 481, 162–170.

Izumi, K., Miyaji, T., Tanabe, K., 2012. Early Toarcian (Early Jurassic) oceanic anoxic event recorded in the shelf deposits in the northwestern Panthalassa: evidence from the Nishinakayama formation in the Toyora area, west Japan. Palaeogeography, Palaeoclimatology, Palaeoecology 15–316, 100–108.

Jenkyns, H. C., 1985. The Early Toarcian and Cenomanian-Turonian anoxic events in Europe: comparisons and contrasts. Geologische Rundschau 74, 505–518.

Jenkyns, H. C., 1988. The Early Toarcian (Jurassic) Anoxic Event: stratigraphic, sedimentary and geochemical evidence. American Journal of Science 288, 101–151.

Jenkyns, H. C., 2003. Evidence for rapid climate change in the Mesozoic–Palaeogene greenhouse world. Philosophical Transactions of the Royal Society of London, Series A 361, 1885–1916.

Jenkyns, H. C., 2010. Geochemistry of oceanic anoxic events. Geochemistry, Geophysics, Geosystems 11, Q03004, doi: 10.1029/2009GC002788.

Jenkyns, H. C., 2020. The demise and drowning of Early Jurassic (Sinemurian) carbonate platforms: stratigraphic evidence from the Italian peninsula, Sicily and Spain. In: L'Eredità scientifica di Paolo Scandone, Atti dei Convegni Lincei 335, 55–82.

Jenkyns, H. C., Clayton, C. J., 1986. Black shales and carbon isotopes in pelagic sediments from the Tethyan Lower Jurassic. Sedimentology 33, 87–106.

Jenkyns, H. C., Clayton, C. J., 1997. Lower Jurassic epicontinental carbonates and mudstones from England and Wales: chemostratigraphic signals and the early Toarcian anoxic event. Sedimentology 44, 687–706.

Jenkyns, H. C., Gröcke, D. R., Hesselbo, S. P., 2001. Nitrogen isotope evidence for water mass denitrification during the early Toarcian (Jurassic) oceanic anoxic event. Paleoceanography 16, 593–603.

Jenkyns, H. C., Jones, C. E., Gröcke, D. R., Hesselbo, S. P., Parkinson, D. N., 2002. Chemostratigraphy of the Jurassic System: applications, limitations and implications for palaeocenography. Journal of the Geological Society 159, 351–378.

Jenkyns, H. C., MacFarlane, S., 2021. The chemostratigraphy and environmental significance of the Marlstone and Junction Bed (Beacon Limestone, Toarcian, Lower Jurassic, Dorset, UK). Geological Magazine, doi: 10.1017/S0016756821000972.

Kafousia, N., Karakitsios, V., Jenkyns, H. C., Mattioli, E., 2011. A global event with a regional character: the Early Toarcian Oceanic Anoxic Event in the Pindos Ocean (northern Peloponnese, Greece). Geological Magazine 148, 619–631.

Kafousia, N., Karakitsios, V., Mattioli, E., Kenjo, S., Jenkyns, H. C., 2014. The Toarcian Oceanic Anoxic Event in the Ionian Zone, Greece. Palaeogeography, Palaeoclimatology, Palaeoecology 393, 135–145.

Kemp, D. B., Coe, A. L., Cohen, A. S., Schwark, L., 2005. Astronomical pacing of methane release in the Early Jurassic period. Nature 437, 396–399.

Kemp, D. B., Selby, D., Izumi, K., 2020. Direct coupling between carbon release and weathering during the Toarcian oceanic anoxic event. Geology 48, 976–980.

Kolonic, S., Wagner, T., Forster, A., Sinnighe Damsté, J. S., Waslworth-Bell, B., Erba, E., Turgeon, S., Brumsack, H.-J., Chellai, E. H., Tsikos, H., Kuhnt, W., Kuypers, M. M. M., 2005. Black shale deposition on the northwest African Shelf during the Cenomanian//Turonian oceanic anoxic event: Climate coupling and global organic carbon burial. Paleoceanography 20, PA1006, doi: 10.1029/2003PA000950.

Korte, C., Hesselbo, S. P., 2011. Shallow marine carbon and oxygen isotope and elemental records indicate icehouse-greenhouse cycles during the early Jurassic. Paleoceanography 26, PA4219, doi: 10.1029/2011PA002160.

Krenker, F.-N., Lindström, S., Bodin, S., 2019. A major sea-level drop briefly precedes the Toarcian oceanic anoxic event: implication for Early Jurassic climate and carbon cycle. Scientific Reports 9, 12518, doi: 10.1038/s41598-019-48956-x.

Leng, M. J., Marshall, J. D., 2004. Palaeoclimate interpretation of stable isotope data from lake sediment archives. Quaternary Science Reviews 23, 811–831.

Littler, K., Hesselbo, S. P., Jenkyns, H. C., 2010. A carbon-isotope perturbation at the Pliensbachian–Toarcian boundary: evidence from the Lias Group, NE England. Geological Magazine 147, 181–192.

Marshall, J. D., 1992. Climatic and oceanographic isotopic signals from the carbonate rock record and their preservation. Geological Magazine 129, 143–160.

Maslin, M., Dickson, A. J., 2015. O-Isotopes. In: Harff, J., Meschede, M., Petersen, S., Thiede, J. (Eds.), Encyclopedia of Marine Geosciences, doi: 10.1007/978-94-007-6644-0_81-1.

Mattioli, E., Pittet, B., Bucefalo Palliani, R., Röhl, H.-J., Schmid-Röhl, A., Morettini, E., 2004. Phytoplankton evidence for timing and correlation of palaeoceanographical changes during the Early Toarcian oceanic anoxic event (Early Jurassic). Journal of the Geological Society of London 161, 685–693.

Mattioli, E., Pittet, B., Petitpierre, L., Mailliot, S., 2009. Dramatic decrease of pelagic carbonate production by nannoplankton across the Early Toarcian anoxic event (T-OAE). Global and Planetary Change 65, 134–145.

Mattioli, E., Pittet, B., Suan, G., Mailliot, S., 2008. Calcareous nannoplankton changes across the early Toarcian oceanic anoxic event in the western Tethys. Paleoceanography 23, PA3208, doi: 10.1029/2007PA001435.

Mattioli, M., Pittet, B., 2002. Contribution of calcareous nannoplankton to carbonate deposition: a new approach applied to the Lower Jurassic of Central Italy. Marine Micropaleontology 45, 175–190.

McElwain, J. C., Wade-Murphy, J., Hesselbo, S. P., 2005. Changes in carbon dioxide during an oceanic anoxic event linked to intrusion into Gondwana coals. Nature 435, 479–482.

Müller, T., Jurikova, H., Gutjahr, M., Tomašovych, A., Schlögl, J., Liebetrau, V., Duarte, L. V., Milovský, R., Suan, G., Mattioli, E., Pittet, B., Eisenhauer, A., 2020. Ocean acidification during the early Toarcian extinction event: Evidence from boron isotopes in brachiopods. Geology 48, 1184–1188.

Müller, T., Price, G. D., Bajnai, D., Nyerges, A., Kesjár, D., Raucsik, B., Varga, A., Judik, K., Fekete, J., May, Z., Pálfy, J., 2017. New multiproxy record of the Jenkyns Event (also known as the Toarcian Oceanic Anoxic Event) from the Mecsek Mountains (Hungary): Differences, duration and drivers. Sedimentology 64, 66–86.

Muttoni, G., Erba, E., Kent, D. V., Bachtadse, V., 2005. Mesozoic Alpine facies deposition as a result of past latitudinal plate motion. Nature 434, 59–63.

Oliveira, L. C. V., Rodrigues, R., Duarte, L. V., Lemos, V. B., 2006. Avaliação do potencial gerador de petróleo e interpretação paleoambiental com base em biomarcadores e isótopos estáveis de carbono da seção Pliensbaquiano–Toarciano inferior (Jurássico Inferior) da região de Peniche (Bacia Lusitânica, Portugal). Boletim de Geociencias da Petrobras 14, 207–234.

Pálfy, J., Smith, P. L., 2000. Synchrony between Early Jurassic extinction, oceanic anoxic event, and the Karoo-Ferrar flood basalt volcanism. Geology 28, 747–750.

Pasquini, C., Vercesi, P. L., 2002. Tettonica sinsedimentaria e ricostruzione paleogeografica del margine occidentale dell'Alto dei Corni di Canzo nel Lias inferiore. Memorie della Società Geologica Italiana 57, 107–114.

Percival, L. M. E., Cohen, A. S., Davies, M. K., Dickson, A. J., Hesselbo, S. P., Jenkyns, H. C., Leng, M. J., Mather, T. A., Storm, M. S., Xu, W., 2016. Osmium isotope evidence for two pulses of increased continental weathering linked to Early Jurassic volcanism and climate change. Geology 44, 759–762.

Percival, L. M. E., Witt, M. L. I., Mather, T. A., Hermoso, M., Jenkyns, H. C., Hesselbo, S. P., Al-Suwaidi, A. H., Storm, M. S., Xu, W., Ruhl, M., 2015. Globally enhanced mercury deposition during the end-Pliensbachian extinction and Toarcian OAE: A link to the Karoo–Ferrar Large Igneous Province. Earth and Planetary Science Letters 428, 267–280.

Pittet, B., Suan, G., Lenoir, F., Duarte, L. V., Mattioli, E., 2014. Carbon isotope evidence for sedimentary discontinuities in the lower Toarcian of the Lusitanian Basin (Portugal): Sea level change at the onset of the Oceanic Anoxic Event. Sedimentary Geology 303, 1–14.

Posenato, R., Bassi, D., Trecalli, A., Parente, M., 2018. Taphonomy and evolution of Lower Jurassic lithiotid bivalve accumulations in the Apennine Carbonate Platform (southern Italy). Palaeogeography, Palaeoclimatology, Palaeoecology 489, 261–271.

Remirez, M. N., Algeo, T. J., 2020. Carbon-cycle changes during the Toarcian (Early Jurassic) and implications for regional versus global drivers of the Toarcian oceanic anoxic event. Earth-Science Reviews 209, 103283.

Reolid, M., 2014. Stable isotopes on foraminifera and ostracods for interpreting incidence of the Toarcian Oceanic Anoxic Event in Westernmost Tethys: role of water stagnation and productivity. Palaeogeography, Palaeoclimatology, Palaeoecology 395, 77–91.

Reolid, M., Mattioli, E., Duarte, L. V., Marok, A., 2020. The Toarcian Oceanic Anoxic Event and the Jenkyns Event (IGCP-655 final report). Episodes 43, 833–844.

Reolid, M., Mattioli, E., Nieto, L. M., Rodríguez-Tovar, F. J., 2014. The Early Toarcian Oceanic Anoxic Event in the External Subbetic (Southiberian Paleomargin, Westernmost Tethys): Geochemistry, nannofossil and ichnology. Paleogeography, Paleoclimatology, Paleoecology 411, 79–94.

Röhl, H. J., Schmid-Röhl, A., 2005. Lower Toarcian (Upper Liassic) black shales of the Central European epicontinental basin: a sequence stratigraphic case study from the SW German Posidonia Shale. In: Harris, N. B. (Ed.), The Deposition of Organic-Carbon-Rich Sediments: Models, Mechanisms, and Consequences, Society for Sedimentary Geology (SEPM), Special Publication 82, 165–189.

Röhl, H.-J., Schmid-Röhl, A., Oschmann, W., Frimmel, A., Schwark, L., 2001. The Posidonia Shale (Lower Toarcian) of SW-Germany: an oxygen-depleted ecosystem controlled by sea level and palaeoclimate. Palaeogeography, Palaeoclimatology, Palaeoecology 165, 27–52.

Ruebsam, W., Al-Husseini, M., 2020. Calibrating the Early Toarcian (Early Jurassic) with stratigraphic black holes (SBH). Gondwana Research 82, 317–336.

Ruebsam, W., Mayer, B., Schwark, L., 2019. Cryosphere carbon dynamics control early Toarcian global warming and sea level evolution. Global and Planetary Change 172, 440–453.

Ruebsam, W., Reolid, M., Sabatino, N., Masetti, D., Schwark, L., 2020. Molecular paleothermometry of the early Toarcian climate perturbation. Global and Planetary Change 195, 103351.

Sabatino, N., Neri, R., Bellanca, A., Jenkyns, H. C., Baudin, F., Parisi, G., Masetti, D., 2009. Carbon-isotope records of the Early Jurassic (Toarcian) oceanic anoxic event from the Valdorbia (Umbria-Marche Apennines) and Monte Mangart (Julian Alps) sections: palaeoceanographic and stratigraphic implications. Sedimentology 56, 1307–1328.

Sabatino, N., Neri, R., Bellanca, A., Jenkyns, H. C., Masetti, D., Scopelliti, G., 2011. Petrography and high-resolution geochemical records of Lower Jurassic manganese-rich deposits from Monte Mangart, Julian Alp. Palaeogeography, Palaeoclimatology, Palaeoecology 299, 97–109.

Sabatino, N., Vlahović, I., Jenkyns, H. C., Scopelliti, G., Neri, R., Prtoljan, B., Velić, I., 2013. Carbon-isotope record and palaeoenvironmental changes during the early Toarcian oceanic anoxic event in shallow-marine carbonates of the Adriatic Carbonate Platform in Croatia. Geological Magazine 150, 1085–1102.

Santantonio, M., Carminati, E., 2011. The Jurassic rifting evolution of the Apennines and Southern Alps (Italy): Parallels and differences. Bulletin of the Geological Society of America 124, 468–484.

Schlanger, S. O., Jenkyns, H. C., 1976. Cretaceous oceanic anoxic events: causes and consequences. Geologie en Mijnbouw 55, 179–184.

Schouten, S., van Kaam-Peters, H. M. E., Rijpstra, W. I. C., Schoell, M., Sinninghe Damsté, J. S., 2000. Effects of an oceanic anoxic event on the stable carbon isotopic composition of early Toarcian carbon. American Journal of Science 300, 1–22.

Scotese, C. R., 2011. The PALEOMAP Project PaleoAtlas for ArcGIS, Volume 3, Jurassic and Triassic Paleogeographic and Plate Tectonic Reconstructions, version (9.2r). PALEOMAP Project, Arlington, Texas.

Storm, M. S., Hesselbo, S. P., Jenkyns, H. C., Ruhl, M., Ullmann, C. V., Xu, W., Leng, M. J., Riding, J. B., Gorbanenko, O., 2020. Orbital pacing and secular evolution of the Early Jurassic carbon cycle. Proceedings of the National Academy of Sciences 117, 3974–3982.

Suan, G., Mattioli, E., Pittet, B., Lécuyer, C., Suchera-Marx, B., Duarte, L. V., Philippe, M., Reggiani, L., Martineau, F., 2010. Secular environmental precursor to Early Toarcian (Jurassic) extreme climate changes. Earth and Planetary Science Letters 290, 448–458.

Suan, G., Mattioli, E., Pittet, B., Mailliot, S., Lécuyer, C., 2008. Evidence for major environmental perturbation prior to and during the Toarcian (Early Jurassic) oceanic anoxic event from the Lusitanian Basin, Portugal. Paleoceanography 23, PA1202, doi: 10.1029/2007PA001459.

Svensen, H. H., Planke, S., Chevallier, L., Malthe-Sørenssen, A., Corfu, F., Jamtveit, B., 2007. Hydrothermal venting of greenhouse gases triggering Early Jurassic global warming. Earth Planet. Sci. Lett. 256, 554–566.

Them, T. R., Gill, B. C., Selby, D., Gröcke, D. R., Friedman, R. M., Owens, J. D., 2017. Evidence for rapid weathering response to climatic warming during the Toarcian Oceanic Anoxic Event. Scientific Reports 7, 5003, doi: 10.1038/s41598-017-05307-y.

Tintori, A., 1977. Toarcian fishes from the Lombardy Basin. Bollettino della Società Paleontologica Italiana 16, 143–152.

Trabucho-Alexandre, J., Dirkx, R., Veld, H., Klaver, G., De Boer, P., 2012. Toarcian black shales in the Dutch Central Graben: record of energetic, variable depositional conditions during an oceanic anoxic event. Journal of Sedimentary Research 82, 104–120.

Trecalli, A., Spangenberg, J., Adatte, T., Föllmi, K. B., Parente, M., 2012. Carbonate platform evidence of ocean acidification at the onset of the early Toarcian oceanic anoxic event. Earth and Planetary Science Letters 357–358, 214–225.

Tremolada, F., van de Schootbrugge, B., Erba, E., 2005. Early Jurassic schizosphaerellid crisis in Cantabria, Spain: Implications for calcification rates and phytoplankton evolution across the Toarcian oceanic anoxic

event. Paleoceanography 20, PA2011, doi: 10.1029/2004PA001120.

Tsikos, H., Jenkyns, H. C., Walsworth-Bell, B., Petrizzo, M. R., Forster, A., Kolonic, S., Erba, E., Premoli Silva, I., Baas, M., Wagner, T., Sinninghe Damsté, J. S., 2004. Carbon-isotope stratigraphy recorded by the Cenomanian–Turonian Oceanic Anoxic Event: correlation and implications based on three key localities. Journal of the Geological Society London 161, 711–719.

Ullmann, C. V., Hesselbo, S. P., Korte, C., 2013. Tectonic forcing of Early to Middle Jurassic seawater Sr/Ca. Geology 41, 211–1214.

van Breugel, Y., Baas, M., Schouten, S., Mattioli, E., Damsté, J. S. S., 2006. Isorenieratane record in black shales from the Paris Basin, France: Constraints on recycling of respired CO_2 as a mechanism for negative carbon isotope shifts during the Toarcian oceanic anoxic event. Paleoceanography, 21, PA4220, https://doi.org/10.1029/2006PA001305.

Visentin, S., Erba, E., 2021. High-resolution calcareous nannofossil biostratigraphy 1 across the Toarcian Oceanic Anoxic Event in northern Italy: clues from the Sogno and Gajum Cores (Lombardy Basin, Southern Alps). Rivista Italiana di Paleontologia e Stratigrafia 127, 539–556.

Visentin, S., Erba, E., Mutterlose, J., 2021. Bio- and chemostratigraphy of the Posidonia Shale: a new database for the Toarcian Anoxic Event from northern Germany. Newsletters on Stratigraphy, doi: 10.1127/nos/2021/0658.

Wagner, T., Hofmann, P., Flögel, S., 2013. Marine black shale deposition and Hadley Cell dynamics: A conceptual framework for the Cretaceous Atlantic Ocean. Marine and Petroleum Geology 43, 222–238.

Winterer, E. L., 1998. Paleobathymetry of Mediterranean Tethyan Jurassic pelagic sediments. Memorie della Società Geologica Italiana 53, 97–131.

Winterer, E. L., Bosellini, A., 1981. Subsidence and sedimentation on Jurassic passive continental margin, Southern Alps, Italy. American Association of Petroleum Geologists Bulletin 65, 394–421.

Woodfine, R. G., Jenkyns, H. C., Sarti, M., Baroncini, F., Violante, C., 2008. The response of two Tethyan carbonate platforms to the early Toarcian (Jurassic) oceanic anoxic event: environmental change and differential subsidence. Sedimentology 55, 1011–1028.

Xu, W., Ruhl, M., Jenkyns, H. C., Hesselbo, S. P., Riding, J. B., Selby, D., Naafs, B. D. A., Weijers, J. W. H., Pancost, R. D., Tegelaar, E., Idiz, E., 2017. Carbon sequestration in an expanded lake system during the Toarcian oceanic anoxic event. Nature Geoscience 10, 129–134.

Xu, W., Ruhl, M., Jenkyns, H. C., Leng, M. J., Huggett, J. M., Minisini, D., Ullmann, C. V., Riding, J. B., Weijers, J. W., Storm, M. S., Percival, L. M., 2018. Evolution of the Toarcian (Early Jurassic) carbon-cycle and global climatic controls on local sedimentary processes (Cardigan Bay Basin, UK). Earth and Planetary Science Letters 484, 396–411.

Manuscript received: June 18, 2021
Revisions required: July 23, 2021
Revised version received: November 12, 2021
Manuscript accepted: November 15, 2021

The pdf version of this paper includes an electronic supplement

Please save the electronic supplement contained in this pdf-file by clicking the blue frame above. After saving rename the file extension to .zip (for security reasons Adobe does not allow to embed .exe, .zip, .rar etc. files).

Table of contents – Electronic Supplementary Material (ESM)

Supplementary material consists of isotopic data ($\delta^{13}C_{carb}$, $\delta^{13}C_{org}$, $\delta^{18}O_{carb}$), $CaCO_3$ content and Total Organic Carbon (TOC) for the Sogno and Gajum cores.